A Reference Section for the Otavi Group (Damara Supergroup) in Eastern Kaoko Zone near Ongongo, Namibia

P.F. Hoffman[1,2,*], S.B. Pruss[3], C.L. Blättler[4], E.J. Bellefroid[5] & B.W. Johnson[6]

[1]*School of Earth & Ocean Sciences, University of Victoria, Victoria, BC, Canada, V8P 5C2*
[2]*Department of Earth & Planetary Sciences, Harvard University, Cambridge, MA 02138, USA*
[3]*Department of Geosciences, Smith College, Northampton, MA 01065, USA*
[4]*Department of Geophysical Sciences, University of Chicago, Chicago, IL 60637, USA*
[5]*Department of Earth & Planetary Sciences, McGill University, Montreal, QC, Canada, H3A 0E8*
[6]*Department of Geological & Atmospheric Sciences, Iowa State University, Ames, IA 50011-1027, USA*
** 1216 Montrose Ave., Victoria, BC, Canada, V8T 2K4. email: <paulfhoffman@gmail.com>*

Abstract : A reference section for the Otavi Group (Damara Supergroup) in the East Kaoko Zone near Ongongo is proposed and described. The section is easily accessible, well exposed, suitable for field excursions, and well documented in terms of carbonate lithofacies, depositional sequences and stable-isotope chemostratigraphy. The late Tonian Ombombo Subgroup is 355 m thick above the basal Beesvlakte Formation, which is not included in the section due to poor outcrop and complex structure. The early-middle Cryogenian Abenab Subgroup is 636 m thick and the early Ediacaran Tsumeb Subgroup is 1020 m thick. While the section is complete in terms of formations represented, the Ombombo and lower Abenab subgroups have defined gaps due to intermittent uplift of the northward-sloping Makalani rift shoulder. The upper Abenab and Tsumeb subgroups are relatively thin due to erosion of a broad shallow trough during late Cryogenian glaciation and flexural arching during post-rift thermal subsidence of the carbonate platform.

Key Words : Neoproterozoic; carbonate platform; carbon isotopes; Cryogenian; Ediacaran

To cite this paper : Hoffman, P.F., Pruss, S.B., Blättler, C.L., Bellefroid, E.J. & Johnson, B.W. 2021. A Reference Section for the Otavi Group (Damara Supergroup) in Eastern Kaoko Zone near Ongongo, Namibia. *Communications of the Geological Survey of Namibia*, **23**, 1-25.

Introduction

The Otavi Group (Fig. 1) is a folded neritic carbonate succession of Neoproterozoic age. In northern Namibia, it is 1.5-3.5 km thick and covers the Congo craton (Northern Platform) east of the Kaoko belt and north of the Damara belt (Miller, 2008). Continuations of the same former carbonate platform occur in the West Congo and Zambian fold belts (Miller, 2013; Delpomdor *et al.* 2016; Cailteaux & De Putter, 2019) as well as in subsurface in the Congo Basin (Kadima *et al.* 2011). The original extent of the shallow-marine carbonate bank was on the order of 5 million square kilometres.

The type area of the Otavi Group is the Otavi Mountainland (SACS, 1980; Hedberg, 1979; King, 1994; Kamona & Günzel, 2007; Miller, 2008). Regrettably, the formations defined in that area (Fig. 1E) were detailed only in unpublished reports (Söhnge, 1953, 1957). There are few modern descriptions of the carbonate sedimentology (Krüger, 1969; Hegenberger, 1987; Bechstädt *et al.* 2009; Delpomdor *et al.* 2018), and existing stable isotope data from the Otavi Mountainland have low stratigraphic resolution (Kaufman *et al.* 1991) except for the youngest formation (Cui *et al.* 2018). Moreover, the oldest of three subgroups making up the revised Otavi Group (Hoffmann & Prave, 1996) is not preserved in the Otavi Mountainland (Fig. 1).

Major upgrades of vehicle route D3710 (Fig. 2) made accessible one of the most complete and conveniently exposed sections of the Otavi Group (2.02 km) in the Eastern Kaoko Zone (Miller, 2008). The top of the section is located 2.2 km east of the spring at Ongongo, 5 km north

of route C43 at Warmquelle (Fig. 2). The purpose of this paper is to present a composite section from Ongongo as a reference section for the Otavi Group in the western part of the platform. As a 2-3-day field excursion, it complements the correlative foreslope section (Swakop Group) at Fransfontein, 170 km to the southeast (Hoffman *et al.* 2021). High-resolution carbonate $\delta^{13}C$ and $\delta^{18}O$ records have been obtained from the Ongongo section and its basin-scale setting is well documented (Hoffman *et al.* 2021). A field guide for the Ongongo section with illustrations different from those in this paper is available as supplementary on-line information SOI S3.12, appended to Hoffman *et al.* (2021).

Structure

The Ongongo section (Fig. 3) is exposed on the western limb of a doubly-plunging anticlinal culmination. The structural culmination is situated at the southern tip (lateral tip-line) of an eastward-vergent thin-skinned thrust-stack exposed in oblique section (Fig. 2). A little over 12 km north-northeast of the culmination, basal Devede Formation is thrust over middle Elandshoek Formation (Fig. 1), a stratigraphic duplication of 1.4 km. The thrust is rooted in a detachment zone that is coextensive with the marly and argillaceous Beesvklate Formation (Fig. 1), exposed in a nest of possible sheath folds north of Okakuyu (Fig. 2).

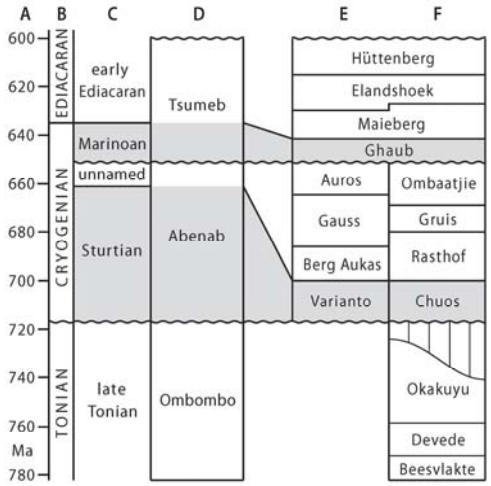

Figure 1. Geologic time scale and Otavi Group formations and subgroups in the Otavi Mountainland and Eastern Kaoko zone. (A) Age in 10^6 years before present (Ma). (B) Periods (Gradstein *et al*. 2012; Shields-Zhou *et al*. 2016). (C) Epochs, with panglacial (snowball) epochs indicated by grey shade. (D) Subgroups of Otavi Group (SACS, 1980; Hoffmann & Prave, 1996). (E) Formations as defined in the Otavi Mountainland (Söhnge, 1957; Hedberg, 1979; SACS, 1980; King, 1994; Hoffmann & Prave, 1996). (F) Formations as defined in the Eastern Kaoko zone (Hedberg, 1979; Hoffman & Halverson, 2008; Hoffman *et al*, 2021). Note that the early Ediacaran and unnamed middle Cryogenian inter-snowball epoch are expanded in E and F relative to the time scale in A-D. Epoch time boundaries: early Cryogenian (Sturtian snowball onset) at 717 Ma (Macdonald *et al*. 2018; MacLennan *et al*. 2018; Lan *et al*. 2020); middle Cryogenian (Sturtian snowball termination) at 661 Ma (Rooney *et al*. 2015, 2020); late Cryogenian (Marinoan snowball onset) at 651 Ma (Prave *et al*. 2016; Bao *et al*. 2018; Nelson *et al*. 2021); early Ediacaran (Marinoan snowball termination) at 635 Ma (Rooney *et al*, 2015; Zhou *et al*, 2019). Top of the Otavi Group is constrained to be ≤600 Ma by D1 metamorphic ($^{39}Ar/^{40}Ar$ phengite) ages in Otavi Group-correlative Swakop Group in the Northern Damara zone (Lehmann *et al*. 2016). The top of the Devede Fm is 760 Ma (Halverson *et al*, 2005; Hoffman *et al*, 2021) based on U-Pb (ID-TIMS) ages for igneous zircon from an airborne volcanic ash layer 37 km NNW of the Ongongo section (Fig. 2).

The thin-skinned thrusts and associated short-wavelength (2-3 km) folds (D1) were subsequently deformed by long-wavelength (20-30 km) thick-skinned structures (D2) of oblique NNW-SSE trend. Major D2 structures include the Sesfontein Thrust and the associated Warmquelle footwall syncline (Fig. 2), and Kamanjab basement anticline and its autochthonous cover of Nosib Group arkosic terrestrial clastics. Structural relief in the area (Fig. 2) owes much to the opposing plunges of the first-order D2 structures, Kamanjab anticline and Warmquelle syncline (Guj, 1970; Hedberg, 1979).

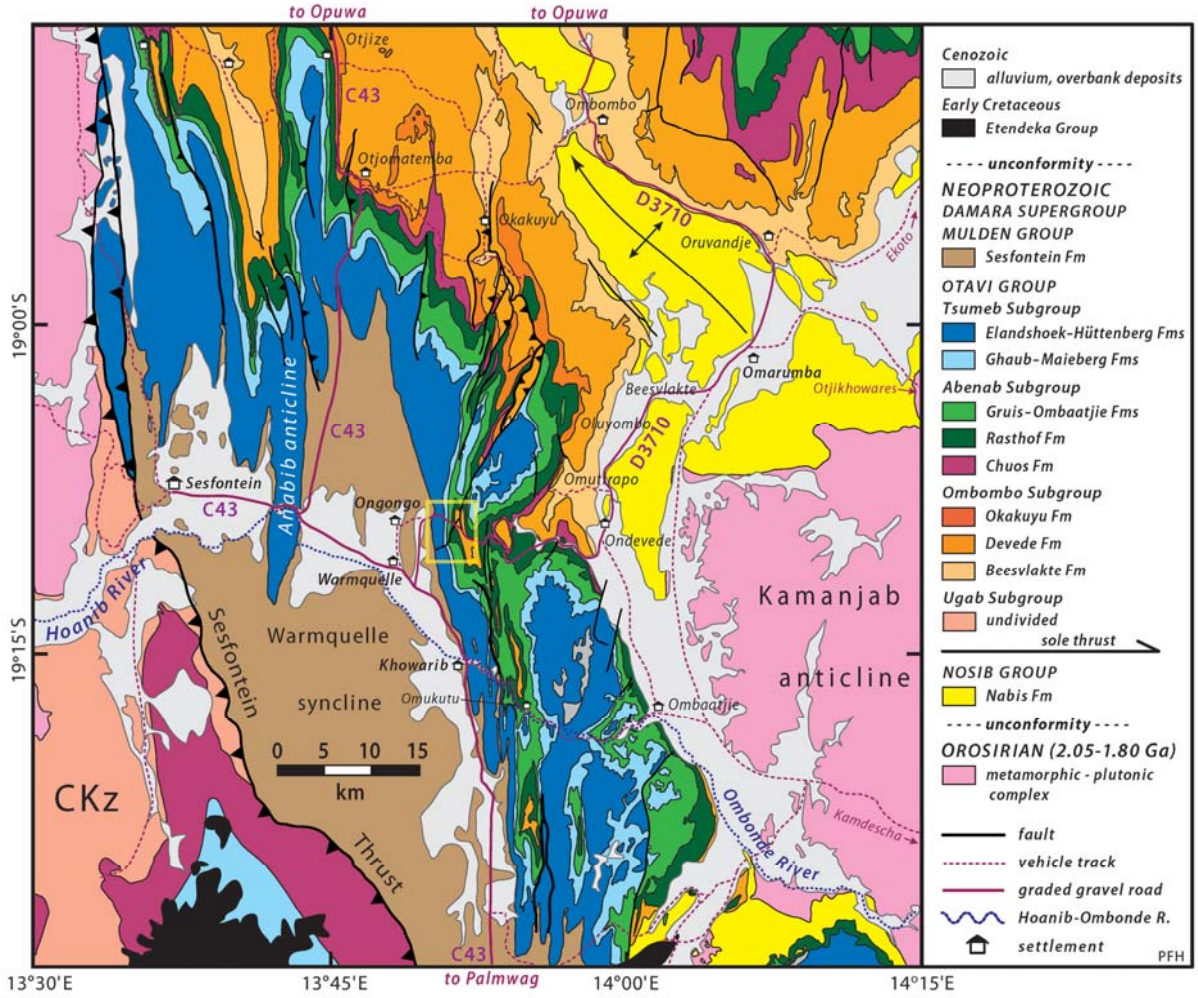

Figure 2. Bedrock geology of the upper Hoanib River area (Hoffman *et al*. 2021). The area of the proposed reference section east of Ongongo is indicated by the yellow box.

The structural culmination east of Ongongo (yellow box, Fig. 2) is aligned with a WSW-ENE line of structural highs. This transverse structural welt is oriented parallel to the Damara belt. A wave train of plunge reversals extends southwards along strike from the culmination east of Ongongo (Fig. 2). These transverse waves could be a far-field response to terminal Damara collision (D3) at ~550 Ma in Southern (Khomas) Zone (Miller, 2008; Goscombe *et al.* 2018).

Basin-scale setting

Ongongo is situated on the inner platform (IPz) of the Otavi Group, 85 km north of the southern foreslope (Hoffman & Halverson, 2008; Hoffman *et al.* 2021). Its distance from the western platform edge is unknown because the Sesfontein Thrust occludes the shelf break. The distance could not have been less than 70 km, assuming 50% W-E tectonic shortening in the train of tight D1 folds and thrusts between Ongongo and the Sesfontein Thrust (Fig. 2).

Subsidence accommodating Otavi Group occurred in two stages: syn-rift and post-rift. The transition coincides with the top of the Gruis Formation (Fig. 1), allowing for minor fault reactivation in the lower Ombaatjie Formation. In terms of stratigraphic thickness at Ongongo, 36% (733 m) of the section is syn-rift and 64% (1285 m) is post-rift. The nearest major rift structure was the northward-tilted dip-slope of Makalani rift-shoulder (Hoffman & Halverson, 2008; Hoffman *et al.* 2021), the crest of which was 70 km south of Ongongo. Terrigenous clastics in the Ombombo and Abenab subgroups at Ongongo were likely derived from the Makalani dip-slope according to palaeocurrents and spatial grain-size variation (Hoffman & Halverson, 2008; Hoffman *et al.* 2021).

Erosional disconformities of glacial origin define the base of the Abenab and Tsumeb subgroups (Fig. 1). Minimum depths of erosion and thicknesses of lost strata can be estimated from subglacial palaeotopographies constructed from measured sections throughout the area (Hoffman *et al.* 2021). The late Tonian Okakuyu Formation (Fig. 1) is relatively thin (45 m) at Ongongo, implying Sturtian erosion of ≥350 m compared with the Okakuyu area 25 km to the north (Fig. 2). Ongongo is situated at the western margin of Omarumba trough (Hoffman *et al.* 2021), a wide shallow NNE-SSW trending glacial trough of Marinoan age. As a result, ≥60 m of uppermost Ombaatjie Formation (Fig. 1) has been lost at Ongongo relative to areas outside the Omarumba trough.

Total post-rift stratigraphic thickness varies significantly S-N across the platform. Thickness minima mark the crest of an arch, the Khowarib arch (Hoffman *et al.* 2021), located ~75 km north of the southern margin and ~30 km south of Ongongo. Thinning over the arch affects the Ombaatjie, Maieberg, Elandshoek and Hüttenberg formations (Fig. 1) in roughly equal proportion (Hoffman *et al.* 2018, 2021). This implies that thinning is not the result of erosion but does reflect spatial variation in long-term subsidence, apparently including a component of lithospheric flexure (e.g. Watts *et al.* 1982). The post-rift succession at Ongongo is 34% thicker (1285 vs 958 m) than the same succession at the crest of the arch, but is only half as thick as sections 60 km to the north - 2560 m at Ohumbameya (Hoffman *et al.* 2018) or 2690 m in the northern Otavi Mountainland (King, 1994). Isopach data compiled by Hedberg (1979) suggest that the Khowarib arch may project eastwards to the southern Otavi Mountainland. South of the arch, the post-rift succession thickens to an estimated 2075 m (61% thicker than at Ongongo) on farm Neuland 541 near the shelf break, 23.5 km west of Outjo.

Location and Access

The Ongongo section is most easily reached from regional route C43 (Fig. 2) between Khorixas and Opuwa. The intersection with D3710 is at 19.1972°S/13.8229°E, 9.0 km NNW of Khowarib. Turn north onto D3710 and proceed 7 km angling toward the near-vertical dolomite before turning eastward into the drainage gap (Fig. 3). The road, as it progresses upstream from bank to bank, descends stratigraphically through 2.02 km of carbonate strata.

There are two structural kinks in the overall west-facing fold limb. At the elevation of the drainage, the short dip reversals are in the Devede and Maieberg formations (Fig. 1). These minor folds may relate to the lateral tip-line of the D1 thrust to the north (Fig. 2).

The riverbed through the section (Fig. 3) is bouldery and not suitable for camping. A cozy and convenient campsite for a small party is located at the small magenta circle in Figure 3. Stop on road D3710 at 19.1457°S/13.8595°E and

turn northeast, perpendicular to the road. Cross the secondary drainage channel and turn left (NNW) onto a seldom-used vehicle track for 0.11 km to the campsite at 19.1449°S/13.8596°E. The entire section is within easy walking distance from this campsite.

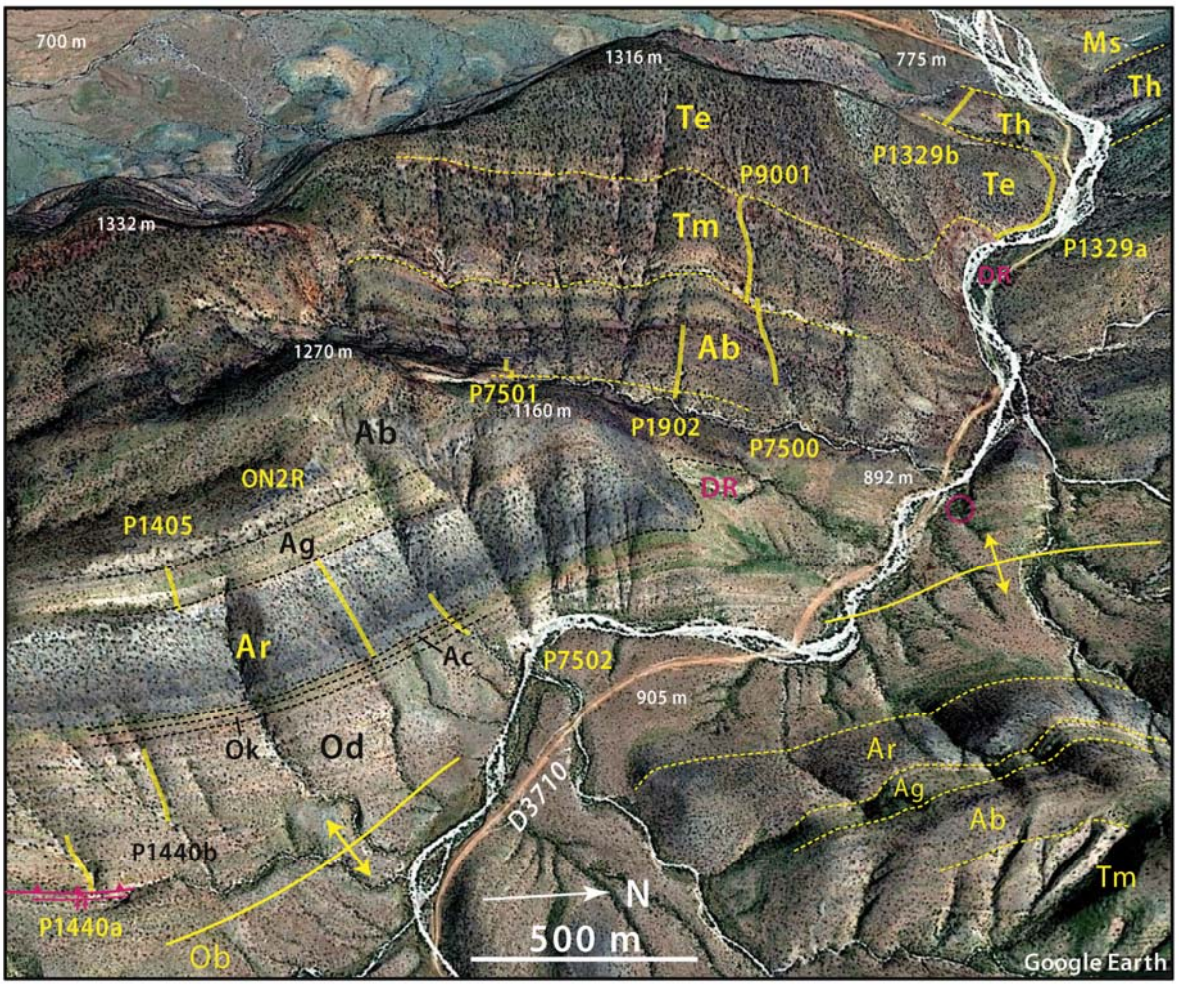

Figure 3. Oblique satellite image looking westward at the proposed Otavi Group reference section on route D3710. Dashed lines indicate formation boundaries and solid yellow lines are the numbered measured sections. Abbreviations (Fig. 1): Ab, Ombaatjie Fm; Ac, Chuos Fm; Ag, Gruis Fm; Ar, Rasthof Fm; DR (magenta), dip reversal; Ms, Sesfontein Fm (Mulden Group); Ob, Beesvlakte Fm; Od, Devede Fm; Ok, Okakuyu Fm; Te, Elandshoek Fm; Th, Hüttenberg Fm; Tm, Maieberg Fm. Magenta circle (centre right) is a convenient campsite. Spot elevations (relative to sea level) in white. Google Earth Image © 2021 Maxar Technologies.

For larger parties, a prepared rest camp at the spring (swimming hole) in Ongongo is located 2.2 km west of the stratigraphic top of the section. At 19.1411°S/13.8370°E on D3710, turn west onto a small dirt track. Follow this track westward, bearing right at forks 0.89 km, 1.53 km and 2.47 km beyond the turnoff. The last fork is at 19.1450°S/13.8155°E. Cross the river at 19.1462°S/13.8130°E and drive north and then northeast for 1.23 km around to the rest camp reception area near 19.1398°S/13.8190°E. Cross back over the river at 19.1405°S/13.8187°E to reach the camping area at 19.1403°S/13.8194°E near the swimming hole on the south side of the river. The campsite can also be reached directly from Warmquelle, 5.8 km to the south on route C43 (Fig. 2).

Lithofacies terminology and carbon isotope excursions

Carbonate lithofacies are categorised as described and illustrated previously (Halverson *et al*. 2002; Hoffman & Halverson, 2008; Hoffman, 2011a; Hoffman *et al*. 2021). 'Rhythmite' is flat-laminated micrite lacking evidence of wave or traction-current action, but may include turbidites and debrites. 'Ribbonite' is thin-bedded (<0.3 m) lutite with wave- or traction-current bedforms including low-angle cross-stratification. 'Stromatolite' refers to laminated microbial-sedimentary structures, typically dendroidal or columnar, occurring both as mounded and tabular bodies. 'Grainstone' is thick-bedded (>0.3 m) arenite, commonly cross-bedded, composed of intraclasts and/or ooids with intergranular void-filling cement and authigenic chert where dolomitized. 'Microbialaminite' refers to microbial-sedimentary deposits with low-relief undulatory laminations characterized by small-scale disconformities, tabular intraclasts, and 'tepee' structures representing polygonal pressure ridges caused by expansive cementation driven by evaporative pumping, indicative of subaerial exposure (Assereto & Kendall, 1978; Kendall & Warren, 1987). In the order given, the five lithofacies are considered to represent a sequence of decreasing water depth at a given location, or a seaward to landward transect across a prograding shelf and coastal system. Microbial lithofacies in the middle Ar2 member of Rasthof Formation (Fig. 1) do not fit comfortably in the general lithofacies scheme. Distinct lithofacies unique in the Otavi Group to Rasthof Formation are described under that formation.

Carbon isotope excursions (CIEs) are significant departures from long-term mean $\delta^{13}C$ values. They are numbered from the base of the Cryogenian and Ediacaran Periods, with odd numbers for negative excursions (lower $\delta^{13}C$) and even numbers for positive excursions (higher $\delta^{13}C$) following Quaternary marine $\delta^{18}O$ stages (Pillans & Gibbard, 2012). Five Cryogenian (Cn1-Cn5) and four Ediacaran (En1-En4) CIEs are recognized in the Otavi Group. Many can be correlated with CIEs defined and named in other regions, as noted below.

Devede and Okakuyu formations (Ombombo Subgroup)

The Ombombo Subgroup (Hoffmann & Prave, 1996) is composed of three formations (Fig. 1), the oldest of which is poorly exposed in the core of the Ongongo anticline and no attempt was made to include it in the measured section (Fig. 4). Where it is best laid out, southeast of Oruvandje (Fig. 2), the Beesvlakte Formation consists of three members: a lower argillite, a middle argillite and a regressive set of upward-shoaling nearshore dolomite cycles (stromatolite, grainstone and intertidal microbialaminite), and an upper marly marble tectonite (Hoffman & Halverson, 2008).

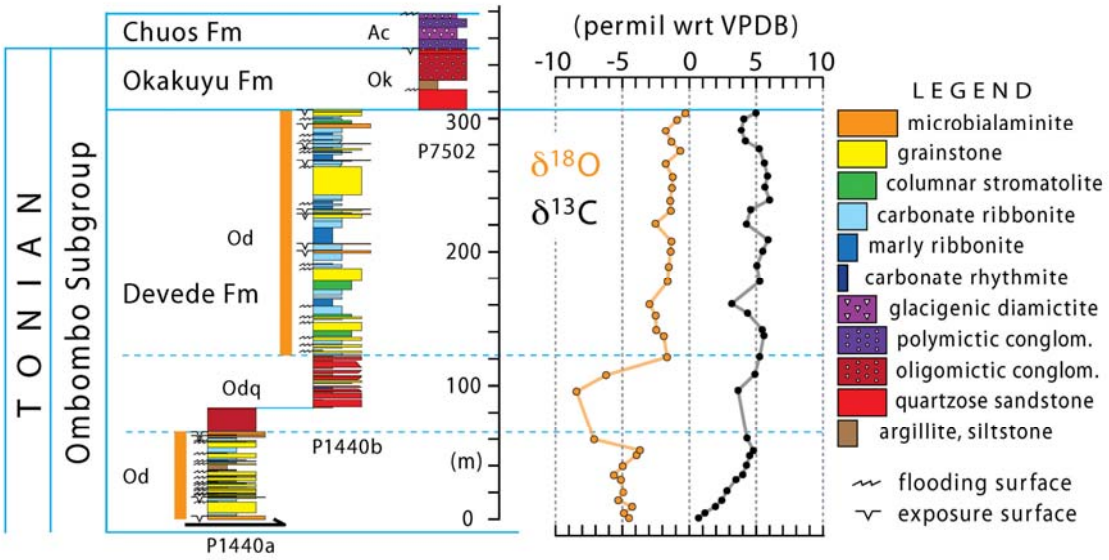

Figure 4. Late Tonian Ombombo Subgroup (Fig. 1) columnar sections P1440a, P1440b and P7502 (Fig. 3), with stable isotope records (Hoffman *et al*. 2021). Abbreviations as in Figure 3. Unit Odq is a northward-tapered siliciclastic tongue in the lower Devede Formation.

Section P1440a (Figs. 3 & 4) begins at 19.1717°S/13.8710°E on the hanging wall of a small eastward-vergent thrust, beneath which is a syncline of lower Devede Formation dolomite. Comparison with adjacent sections suggests that the hanging wall of the thrust at this location is close to the base of the Devede Formation, which is defined as the first dolomite ≥1.0 m thick. The Devede Formation is 310 m thick in P1440, which is a composite of two sections P1440a and b (Figs 3 & 4). Essentially, it is a stack of regressive nearshore dolomite cycles with a member (Odq) rich in siliciclastic (quartz-chert) rudite and arenite between 85 and 126 m stratigraphically above the datum. This mappable wedge of clastics thickens southward toward the Makalani rift shoulder and consists of resistant debris eroded from uplifted quartzarenite (Nabis Formation) and authigenic chert from the lower Devede dolomite (Hoffman & Halverson, 2008). It records SSE-down rift-faulting on the Makalani structure in early Devede Formation time with rift-shoulder uplift as an isostatic response. At the base of the siliciclastic member in P1440a is a 17-m-thick roundstone conglomerate, the top of which is easily walked out linking sections P1440a and b (Fig. 3). The top of the section 'a' is at 19.1724°S/13.8698°E and the base of section 'b' is at 19.1697°S/13.8693°E. The conglomerate contains clasts of quartz, quartzite, amphibolite and granodiorite, indicating formerly exposed basement on the Makalani dip-slope.

In total, the Devede Formation in P1440 contains approximately 52 depositional cycles, yielding an average thickness of 6.0 m per cycle. The cycles are strongly asymmetric with condensed transgressions and fulsome regressions in the (complete) sequence marly ribbonite (wavy dololutite), ribbonite, stromatolite, cherty grainstone (beds ≥0.4 m) and microbialaminite. Twelve of the cycles end at evident subaerial exposure surfaces (tepee structure, Assereto & Kendall, 1978; Kendall & Warren, 1987) and the rest at marine flooding surfaces (36) or erosive scours (4). There are eleven columnar stromatolite beds ranging from 0.3 to 6.8 m thick (average 1.5 m), the more developed of which exhibit divergent to prone branching typical of the morphotype *Tungussia* Semikhatov (Hofmann, 1969). Commonly pale pinkish in colour, the bedding-parallel branches give these stromatolite beds a nodular appearance in outcrop.

In most other sections, there is a 150-m-thick interval dominated by pink *Tungussia* stromatolite biostromes near the top of the Devede Formation (Hoffman & Halverson, 2008; Hoffman *et al*. 2021). This interval is missing at

Ongongo. Because the Devede Formation at Ongongo is 100-180 m thinner than other sections (n=4) within 20 km distance (to the northeast, Fig. 2), erosion beneath the disconformity at the base of the overlying Okakuyu Formation (Fig. 4) is the simplest explanation for the missing thick stromatolite biostrome interval. The disconformity has 4.0 m of local relief at the top of section P1440b (19.1701°S/13.8676°E).

The Okakuyu Formation is only 5.6-9.6 m thick in section P1440b, so a thicker (45.4 m) section at P7502 (Fig. 3) was utilized in the composite section (Fig. 4). The base of the Okakuyu Fm in P7502 is at 19.1614°S/13.8634°E and the section consists of two units each of quartz-quartzite-chert-pebble conglomerate and cross-bedded sandstone of the same composition, and a single unit of thin-bedded argillaceous siltstone (Fig. 4). The top of the Okakuyu Formation at 19.1615°S/13.8632°E is poorly exposed, but the basal Chuos conglomerate can be distinguished from the underlying Okakuyu conglomerate by the presence of dolomite clasts, more abundant chert clasts and a less well-sorted matrix. Since the Okakuyu Formation is 300-350 m thick 25 km north of Ongongo (Hoffman & Halverson, 2008), we must assume that in the Ongongo section it is ≥85% erosionally truncated beneath the sub-Chuos Formation disconformity/ unconformity. Northward younging toplaps beneath the Okakuyu and Chuos formations suggest repeated late Tonian (post-760 Ma) reactivations of the Makalani rift shoulder.

Chuos and Rasthof formations (Abenab Subgroup)

The Sturtian glacigenic Chuos Formation was measured in section P7502 and its cap-carbonate sequence, the Rasthof Formation was documented in section ON2R (Figs 3 & 5). The Rasthof Formation $\delta^{13}C$ data are from Pruss *et al*. (2010).

The 26-m-thick Chuos Formation consists of two conglomerates, each overlain by diamictite (Fig. 5). Both conglomerates carry clasts of dolomite, chert, quartzite and quartz, the older (7.0 m) being stratified and the younger (6.3 m) fining upward. The diamictites are matrix-supported polymictic rudites with clast types similar to the conglomerates but with the addition of basement granodiorite clasts in the older, thicker (8.8 m) and more massive of the two diamictites. This older diamictite has a mud-rich greywacke matrix and both rounded and angular cobbles. The younger diamictite (3.8 m) is weakly stratified, clast-size graded and Fe-enriched. The base of the Chuos Formation is at 19.1615°S/13.8632°E in P7502 and its top is at 19.1616°S/13.8631°E.

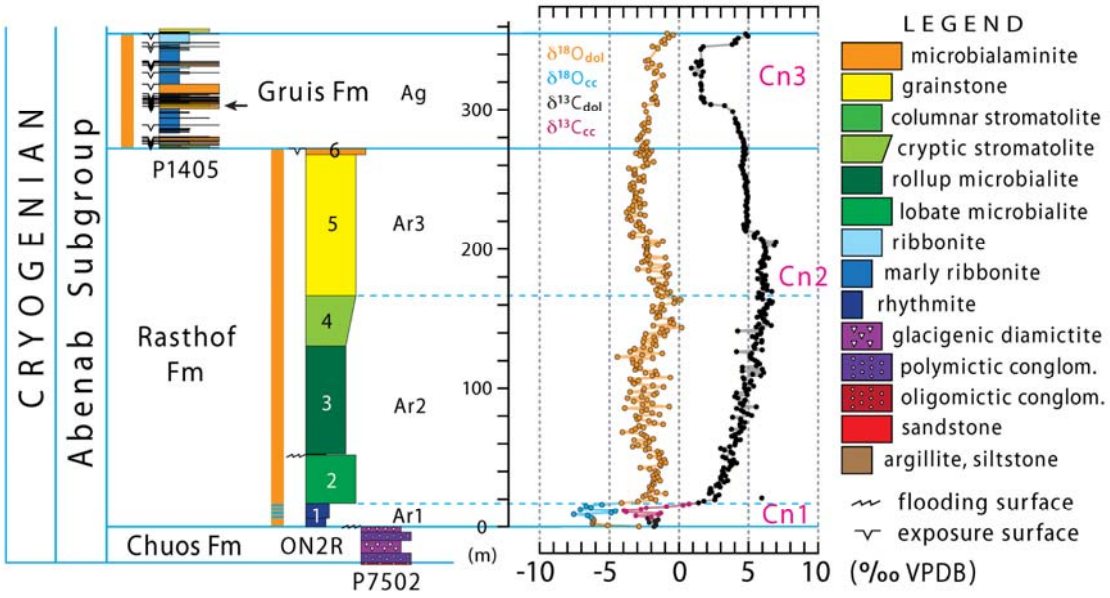

Figure 5. Cryogenian lower Abenab Subgroup (Fig. 1) columnar sections P7502 (Chuos Fm), ON2R (Rasthof Fm) and P1405 (Gruis Fm), with stable isotope records (Hoffman *et al*. 2021). See Figure 3 for section locations. The Rasthof Formation is divisible into three members (Ar1-3) and six lithofacies units (see text). Note colour coding for dolomite (orange and black) and calcite (blue and purple) isotope data points.

The 271.5-m-thick Rasthof Formation is essentially an inflated highstand depositional sequence divided into six lithofacies units (Fig. 5). The deepest-water facies is at the base of the formation and the shallowest is at the top, with but a single flooding surface within the sequence. Much of the postglacial accommodation space required for highstand Rasthof accumulation would have been provided by net Sturtian erosion - 255-305 m of Okakuyu Formation eroded (see previous section) less 26 m of Chuos Formation deposited.

Unit 1 (Ar1, Fig. 5) is 17.0 m thick in section ON2R and consists of dark grey parallel-laminated abiotic dolomite rhythmite with spaced 5-30-cm-thick limestone turbidites and fine-grained debrites in the upper 10 m. Its basal contact with Fe-rich diamictite is knife-sharp, and its upper contact with lobate microbialite (unit 2) is gradational over ~0.5 m.

Unit 2 ('lobate microbialite,' Fig. 5) is 35.0 m thick in ON2R and corresponds to the 'thickly-laminated' facies (Pruss *et al*. 2010; Bosak *et al*. 2011; Dalton *et al*. 2013). A medium grey dolomite, it is a laminated microbialite characterised by 10-20-cm-scale convexities that expand upwards in any fixed direction, climbing obliquely above an inclined zone of tightly deformed laminae with abundant 'chambered' void-filling sparry cement (Pruss *et al*. 2010; Le Ber *et al*. 2013; Wallace *et al*. 2014). In cross-section, these microbial 'lobes' resemble anticlines developed over thrust ramps, but unlike tectonic structures their directions of lateral growth have no preferred azimuth. A possible cause of non-directional compression (constriction) in the horizontal plane is microbial growth expansion, with lobes being an expression of the free surface. Microbial growth expansion has been invoked to explain 'microbial polygons' in productive tidal ponds on the littoral coast of the United Arab Emirates (Lokier *et al*. 2018). Unlike the Persian/Arabian Gulf microbial structures, the 'lobate microbialites' in the Rasthof Formation lack evidence of desiccation or current action. A small percentage of the lobes develop sharp secondary crests that aggrade vertically (Hoffman *et al*. 2021). These are the only suggestions of phototropism in what, from its sequence stratigraphic position, is inferred to be a deep sublittoral environment. An oddity of unit 2 is that from a distance it appears to be

regularly bedded on a 2-m-scale, but at the outcrop this bedding is cryptic.

Unit 3 ('rollup microbialite,' Fig. 5) is 78.5 m thick in ON2R and corresponds to the 'thinly-laminated' facies (Pruss *et al*. 2010; Bosak *et al*. 2011; Dalton *et al*. 2013). Its top is gradational but its base is a prominent flooding surface, underlain by a 20-cm drape of quartzose silty dolomite with low-angle cross-stratification and overlain by 0.6 m of marly dolomite ribbonite. Unit 3 microbialite is a smoothly laminated dolomite which at a distance has the darkest grey colour within the Rasthof Formation (Fig. 3), but which actually consists of alternating dark and light laminae averaging 13 couplets per cm. The dark laminae become paler with stratigraphic height such that the top of unit 3 is less a loss of laminae than a loss of colour contrast.

'Rollups' are the iconic structure in unit 3 and consist of delaminated flaps, generally 2-6 couplets thick, that were folded and refolded on the seafloor (Hoffman *et al*. 1998a; Hoffman & Halverson, 2008; Pruss *et al*. 2010; Bosak *et al*. 2013; Le Ber *et al*. 2013). The rollups indicate that the sediment was cohesive but pliable when folding occurred, presumably because of microbial binding. How the flaps were originally torn is usually conjectural, but in some cases, it is related to intermittent fluid or gas expulsion from neptunian dykes (Pruss *et al*. 2010; Bosak *et al*. 2013; Hoffman *et al*. 2021). Some such dykes are bordered by stacks of flaps that were successively back-flipped away the dyke, flap after flap. The dykes themselves are typically filled by microbialite intraclasts and void-filling cement.

Insoluble residues from samples of units 2 and 3 in ON2R contain variable concentrations of microscopic, organic-rich, regularly-sized, elliptical bodies (110 x 70 μm) and tubular structures, interpreted as the agglutinated tests of protistan heterotrophs (Pruss *et al*. 2010; Bosak *et al*. 2011, 2012; Dalton *et al*. 2013). Biological agglutination of detrital grains is supported by mineralogical investigation of post-Sturtian cap-carbonate sequences in Zambia (Kakontwe Formation) and Mongolia (Tayshir Formation) containing similar microfossils (Moore *et al*. 2017).

Unit 4 is 35 m thick in ON2R and is gradational with units 3 and 5 (Fig. 5). Palimpsest microbial lamination is evident basally and mechanical layering at the top. The term 'cryptic stromatolite' alludes to ghost-like columnar structures in which vertically aggraded cuspate arches are separated by concave 'dish' structures. In other sections, unit 4 contains spaced, mostly non-branching columnar stromatolites with indistinct convex internal laminations and encrusted sidewalls, resembling the morphotype *Boxonia* Korolyuk (Hofmann, 1969).

Unit 5 is 102 m thick in ON2R and consists of light grey dolomite grainstone with low- to high-angle cross-bedding and increasing amounts of authigenic white chert towards the top. Unit 6 is 3.8 m thick and ends at a heavily-silificied sequence boundary beneath which are 1.6 m of dolomite microbialaminite with tepee structures indicating subaerial exposure. The sequence boundary marks a colour change from grey to pink dolomite. In section P1405 (Fig. 5), there are two 0.5-m-thick tepeed microbialaminite horizons 2 and 3 m below the heavily-silicified sequence boundary marking the top of the Rasthof Formation.

Gruis Formation (Abenab Subgroup)

The Gruis Formation (Hedberg, 1979; Hoffman & Halverson, 2008) was measured and sampled in section P1405 (Fig. 3), the base of which is at 19.1688°S/13.8641°E. Recessive, thin-bedded and straw-coloured on exposed surfaces, it differs in almost every respect from the underlying Rasthof Formation. In a total thickness of 114.2 m (Fig. 6) there are no fewer than 40 depositional cycles (2.86 m per cycle), 29 of which end at subaerial exposure surfaces marked by well-developed tepee structures. Not surprisingly, the formation is highly oxidized overall and its dolomite is typically pinkish on fresh surfaces. Marly ribbonite is the most common lithology in aggregate, followed by microbialaminite, ribbonite and grainstone in declining order. A 1.0-m-thick grainstone bed 35 m above the datum (black arrow in Fig. 6) carries fist-size nodules of authigenic white chert. The same chert marker bed is observed at virtually the

same position (±2.0 m) with respect to the $\delta^{13}C$ record (i.e. CIE Cn3 downturn, Fig. 6) over an area the size of Fig. 2, but shifted 30 km eastward (Hoffman *et al*. 2021).

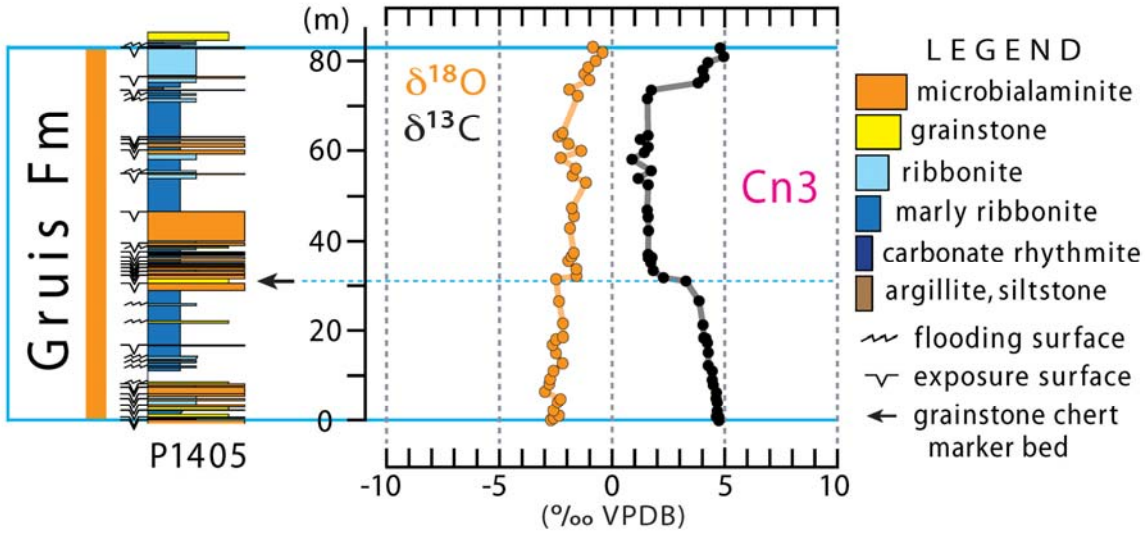

Figure 6. Gruis Formation (Fig. 1) enlarged columnar section and stable isotope record from section P1405 (Fig. 3). Horizontal arrow indicates the nodular chert grainstone marker bed that regionally coincides with the $\delta^{13}C$ downturn of CIE Cn3 (Hoffman *et al*. 2021). Cn3 appears to be a blunted expression of the Tayshir CIE in Mongolia (Johnston *et al*. 2012; Bold *et al*. 2016).

In the terminology of Schlager (2005), the Rasthof Formation was a 'catch-up' sequence and the Gruis Formation a 'keep-up' one. In Rasthof time, sedimentation had to catch-up with subsidence accommodation generated during the 56-Myr Sturtian glaciation when little sedimentation occurred because of the weak hydrologic cycle (Partin & Sadler, 2016). Once it did catch up, at the Rasthof top sequence boundary, it was able to keep pace with subsidence on orbital (cycle?) time scales thereafter. The marly impurity of the Gruis Formation is a distal manifestation of the last major episode in the 100-Myr uplift history of the Makalani rift-shoulder, where 60 km southeast of Ongongo the Gruis Formation oversteps the Rasthof Formation onto the crystalline basement complex and contains ≤150 m of basement-derived alluvial fanglomerate (Hoffman & Halverson, 2008; Hoffman *et al*. in press).

Ombaatjie Formation (Abenab Subgroup)

The $\delta^{13}C/\delta^{18}O$ records from the Ombaatjie Formation (Hoffmann & Prave, 1996; Hoffman & Halverson, 2008) are composites from sections P7501 and P7500 (Figs 3 & 7). The datum for P7501 is at 19.1586°S/13.8548°E where the contact with Gruis Formation is well exposed. Section P7500 begins at 19.1502°S/13.8552°E and ends at the top of the Ombaatjie Formation at 19.1510°S/13.8530°E (Figs 7 & 8A). A complete section (P1902) of the lower Ombaatjie Formation (units b1-b3) was measured but not sampled (Fig. 9B). Eight parallel sections of the upper Ombaatjie Formation (units b4-b8) were measured (two sampled) at Ongongo as a test of km-scale lateral variability of the cycles (Figs 8A & 9A).

The Ombaatjie Formation is an aggradational stack of upward-shoaling depositional cycles. An influx of quartz sand at the base of unit b4 (Fig. 9A), evident from afar as a dark-brown band of desert 'varnish' (Fig. 8A), serves to separate the formation into two natural divisions. Taking section P1902 (Fig. 9B) to represent the lower division (units b1-b3) and P7500 (Fig. 9A) the upper (units b4-b8), gives a total to 27 depositional cycles in 280 m of strata,

for an average cycle thickness of 10.4 m. Comparison with Gruis Formation (2.86 m average cycle) and Elandshoek Formation (7.2 m) suggests rapid acceleration in tectonic subsidence rate between Gruis and Ombaatjie time and a gradual decline in subsidence rate thereafter. While consistent with a transition from rift to post-rift thermal subsidence at the Gruis-Ombaatjie boundary, the relation between cycle thickness and subsidence rate assumes that the same orbital period resonated with depositional cycle dynamics.

Most lower Ombaatjie cycles (12 of 15) end at marine flooding surfaces (i.e. abrupt increases of inferred water depth) above intraclast and/or ooid grainstone (Fig. 9B). In contrast, most upper Ombaatjie cycles (9 of 12) end at subaerial exposure surfaces above microbialaminite with tepees (Fig. 9A). The cycle stack in this area is somewhat regressive overall. Perhaps as a result, the upper Ombaatjie Formation is more thoroughly dolomitized than the lower Ombaatjie (Fig. 7). For this reason, we hesitate to compare cycle thickness between the lower and upper Ombaatjie Formation. Limestone has been preferentially thinned stratigraphically relative to dolomite by tectonic flattening across the steeply-dipping cleavage

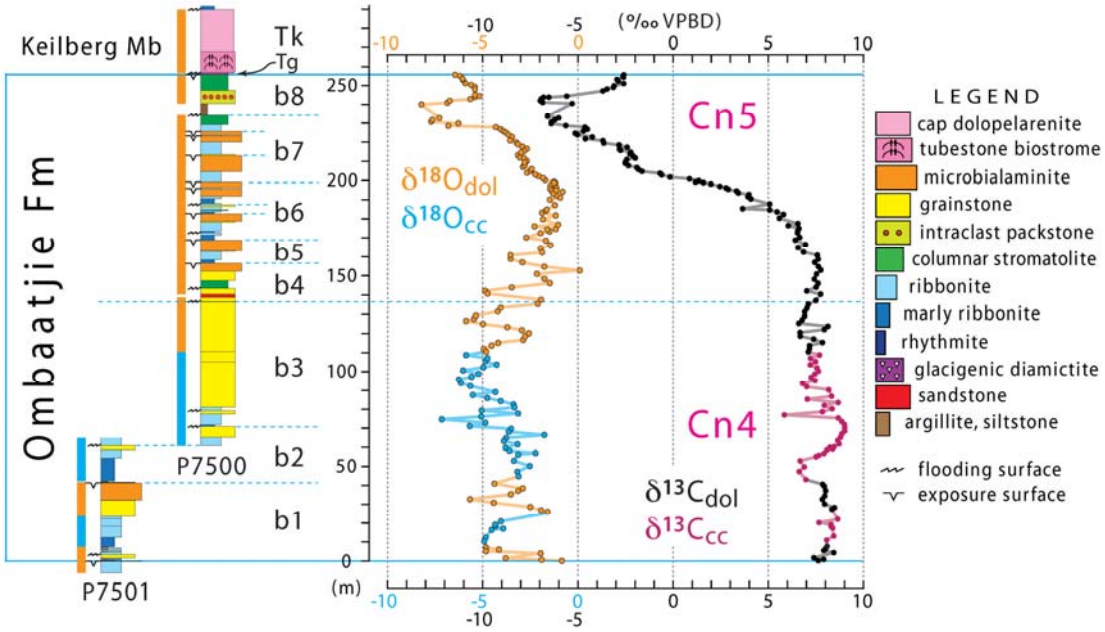

Figure 7. Ombaatjie Formation (Fig. 1) columnar sections P7501 and P7500 (Figs. 3 & 8A), with stable isotope records (Hoffman *et al*. in press). Note offset $\delta^{18}O$ (blue & orange) and $\delta^{13}C$ (black) scales. Dolomite and calcite are colour coded as in Figure 5. The formation is divided into eight units b1-b8 and two members at the base of unit b4 (see text). An unbroken b1-b3 section (without isotope data) is shown in Figure 9B. CIE Cn4 is correlated with Keele peak (Kaufman *et al*. 1997) and Cn5 with Trezona CIE (Rose *et al*. 2012).

Units b7 and b8 are associated with the Cn5 C-isotope excursion (Figs 7 & 9A), which is correlated with the immediate pre-Marinoan Trezona CIE (Halverson *et al*. 2002; Rose *et al*. 2012). Unit b8 and the top of unit b7 are also notable for a proliferation of large (multi-metre) stromatolite mounds composed internally of cm-scale columns with strongly divergent dendroid branching (form-group *Tungussia* Semikhatov, Hofmann, 1969). The stromatolite proliferation was cited as evidence for elevated carbonate saturation in support of a biogeochemical model in which the C-isotope excursion was driven by enhanced rates of anaerobic relative to aerobic respiration, presumably in response to increased delivery of sulfate and/or ferric Fe as electron acceptors (Tziperman *et al*. 2011).

Unit b8 is also notable for the occurrence of 'intraclast packstone' (Fig. 9A). This unusual lithotype is found on the outer and inner platform but only in unit b8 (Hoffman *et al*. in press). It consists of oligomictic rounded granules of Fe-rich carbonate (ankerite) up to a few millimeters in diameter. The coarse grains are set in a fine-grained carbonate mud matrix of similar composition. The packstone is mechanically bedded, even cross-bedded, implying that the muddy matrix was emplaced post-depositionally by infiltration. Authigenic FeS_2 nodules are common and formed after the matrix was emplaced. The palaeoenvironmental significance of intraclast packstone in b8 remains an unsolved mystery, but the Fe-rich carbonate was likely authigenic in origin at its source (i.e. before erosion and redeposition as bedded granules). Enhanced authigenic carbonate production would be consistent with the anaerobic respiration model for CIE Cn5 (Tziperman *et al*. 2011).

Ghaub and Maieberg formations (Tsumeb Subgroup)

The main repository for Marinoan glacial deposits (Ghaub Formation, Hoffmann & Prave, 1996) was on the foreslope of the carbonate platform near the ice grounding zone (Hoffman, 2004, 2011a, b; Domack & Hoffman, 2011). Only scraps of carbonate-clast diamictite, interpreted as lodgement tillite, are found on the glaciated top of the platform (Hoffman *et al*. in press). Of nine sections at Ongongo that cross the Cryogenian-Ediacaran boundary (Fig. 8A), only five preserve any Ghaub Formation (unit Tg, Fig. 9A - P9000 (0.3 m), P9001 (0.2 m), P7500 (≤0.6 m), E1403 (0.8 m) and E1402 (2.4 m). No clast fabric data (Dowdeswell *et al*. 1985) were obtained at Ongongo, but strongly preferred NNE-SSW azimuthal long-axis orientations are documented in Ghaub diamictite 23 km south-southeast of P7500 (Hoffman *et al*. in press). This fabric is compatible with south-southwest-directed Marinoan glacial flow in present coordinates.

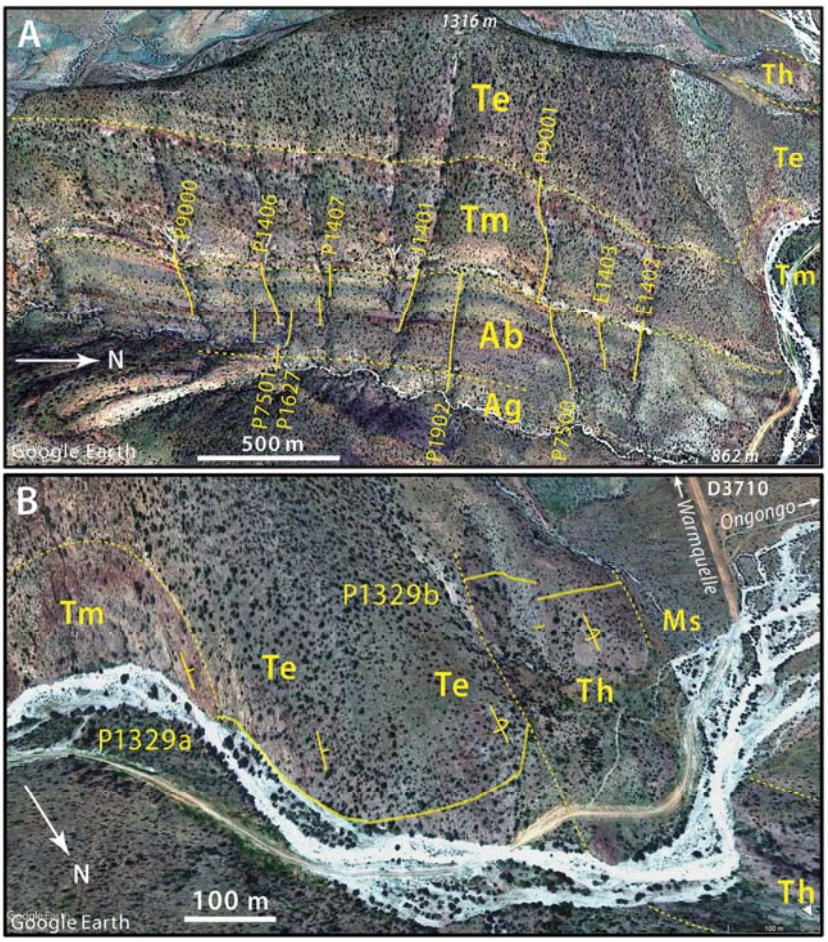

Figure 8. Oblique satellite images: **(A)** Ombaatjie (Ab) and Maieberg (Tm) formation sections (solid yellow) shown in Figures 7, 9 and 10; **(B)** Elandshoek (Te) and Hüttenberg (Th) formation sections shown in Figures 11 and 12. Google Earth Images © 2021 Maxar Technologies.

The basal Ediacaran cap-carbonate sequence (Maieberg Formation, Hoffman & Halverson, 2008) was measured and sampled in two parts: the Keilberg Member (unit Tk) in P7500 and the rest (units Tm2 and Tm3) in P9001 (Figs 3, 8A & 10). The base of the Keilberg Member in P7500 is at 19.1511°S/13.8530°E and the base of Tm2 in P9001 is at 19.1516°S/ 13.8526°E (Figs 8A & 10).

The ever-present Keilberg Member (Hoffmann & Prave, 1996; Hoffman *et al*. 2007) represents the basal Ediacaran cap dolomite observed globally in marine sequences (Knoll *et al*. 2006; Narbonne *et al*. 2012). It is 33.1 m thick in P7500 (30.0 m in P9001) and stands out as a very pale-grey to white flinty dolomite with a palimpsest peloidal texture and a knife-sharp basal contact. The basal 0.5 m is mechanically stratified with low-angle cross-bedding. It is overlain by 5.5 m (P9001) to 10.7 m (P7500) of weakly developed tubestone stromatolite (Hegenberger, 1987; Hoffman, 2011b). Above the stromatolitic interval is peloidal grainstone featuring hummocky cross-stratification (HCS) with low-angle downlaps, but no giant wave ripples or sand volcanoes as occur elsewhere on the platform in the same interval (Allen & Hoffman, 2005; Crockford *et al*. 2021; Hoffman *et al*. in press). In the uppermost Keilberg Member, bedding becomes thin and tabular (Fig. 10). The contact with limestone rhythmite (locally dolomitized) of member Tm2 is well defined, but lacks any evident break in sedimentation. Benthic crystal fans, pseudo-morphic after cm-scale seafloor aragonite cement, begin at the base of Tm2 (e.g. P9001 and

E1403, Fig. 8A) but are never observed in the Keilberg Member. As an upward-deepening sequence, Keilberg Member is interpreted as the relatively expanded transgressive systems tract in the Maieberg depositional sequence (Hoffman & Halverson, 2008; Hoffman, 2011b).

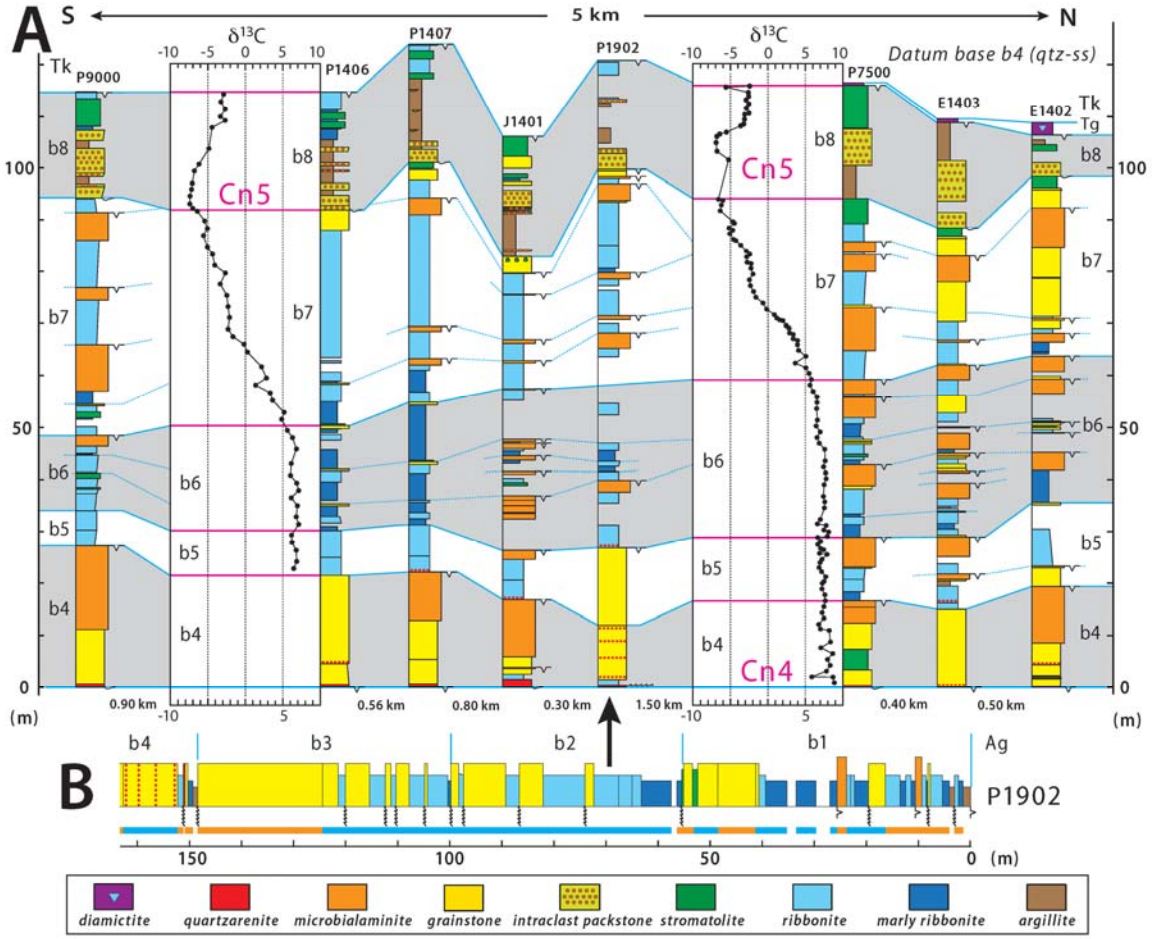

Figure 9. (A) Upper Ombaatjie Formation (units b4-b8) closely-spaced columnar sections (Fig. 8A) with $\delta^{13}C$ records (Hoffman *et al*. in press) from P1406 and P7500 (see Fig. 7 for $\delta^{18}O$ record). **(B)** Lower Ombaatjie Formation (units b1-b3) columnar section P1902 (Fig. 8A).

The middle Tm2 member of the Maieberg Formation (Hoffman *et al*. in press) consists of limestone/dolomite rhythmite and marly rhythmite deposited below storm wave base. It encompasses the maximum flooding and lower highstand parts of the post-Marinoan depositional sequence. It is analogous to the Brachina Formation in South Australia (Preiss & Forbes, 1981), the Sheepbed Formation in northwest Canada (Aitken, 1982), the Guia Formation in southwest Brazil (Nogueira *et al*. 2007) and the C2 (Bulu) Formation of the Schisto-Calcaire Subgroup in the West Congo Supergroup (Delpomdor *et al*. 2016). Benthic crystal fans (former aragonite) occur abundantly in the first 52 m of Tm2 in P9001, which is their maximum development on the inner platform. Spaced prismatic fans ≤16 cm in length (palaeovertical) occur in the lower half of this interval and bunched clusters the size of cabbages in the upper half. Because of tectonic strain, their morphology is better preserved where dolomitized (Fig. 10). On the foreslope and outer margin of the platform, Tm2 crystal fans are

spatially associated with seafloor topography, implicating enhanced vertical mixing in their occurrence (Hoffman & Halverson, 2008; Hoffman, 2011a). At Ongongo, vertical mixing may have been localized by the sidewall of a Marinoan glacial trough (Omarumba Trough, Hoffman *et al*. in press).

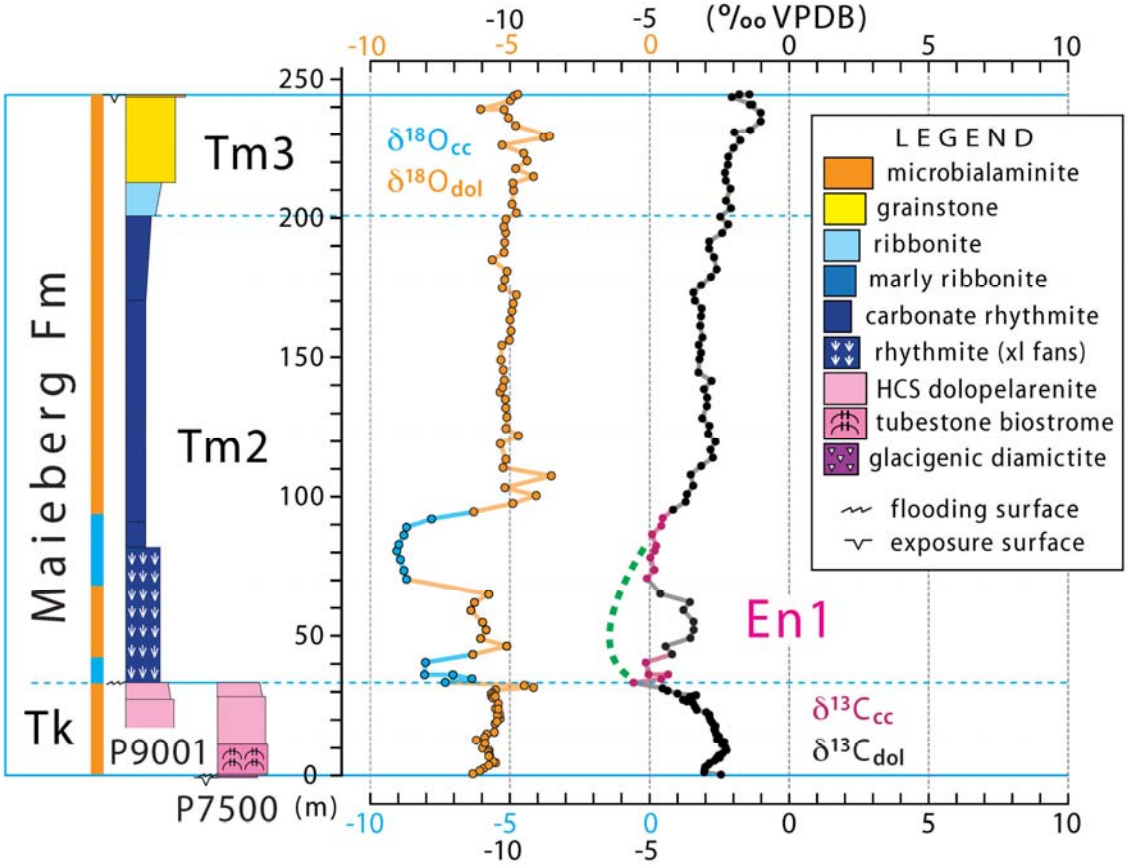

Figure 10. Earliest Ediacaran Maieberg Formation (Fig. 1) columnar section P9001 (Figs. 3 & 8A) with stable isotope records (Hoffman *et al*. in press). Note offset $\delta^{18}O$ (blue & orange) and $\delta^{13}C$ (black) scales. Dolomite and calcite are colour coded as in Figure 5. The formation is divisible into three members Tm1-Tm3. Note dolomite-calcite isotopic fractionations, consistent with low-temperature equilibrium fractionations (Friedman & O'Neil, 1977), not observed in Ombaatjie Formation (Fig. 7). Green dashed line indicates $\delta^{13}C$ trajectory in undolomitized lower Tm2 sections (Hoffman *et al*. in press).

The Maieberg Formation is the only formation in the Otavi Group that exhibits consistent $\delta^{13}C$ and $\delta^{18}O$ fractionations between coexisting dolomite and calcite (Hoffman, 2011b). The lower part of Tm2 includes the nadir of the first Ediacaran negative C-isotope excursion En1 (Fig. 10). P9001 is interesting because En1, which is normally expressed in limestone, is partly dolomitized. Both $\delta^{18}O$ and $\delta^{13}C$ are shifted to heavier values where dolomitized (Fig. 10). Similar shifts are associated with dolomitization of the post-Marinoan cap-carbonate sequence (Ol Formation) of the Zavkhan terrane in western Mongolia (Bold *et al*. 2020).

The Upper Maieberg member Tm3 begins with the first bedforms indicating wave or traction current action. They are preceded in upper Tm2 by fine-grained debrites. Tm3 dolomite ribbonite grades upwards into massive or cross-bedded grainstone (Fig. 10). Authigenic silicification increases in intensity upwards towards the terminal sequence boundary above a thin veneer of microbialaminite with tepees.

The Maieberg Formation is exceptionally thick as a single transgressive-highstand depositional sequence without higher-order cycles or parasequences. This reflects a large accommodation generated through rapid (early post-rift) tectonic subsidence and net erosion of the platform during Marinoan glaciation (Hoffman *et al*. 1998a, b). In contrast, because of its location near the crest of the Khowarib arch (Hoffman *et al*. in press) the Maieberg Formation is relatively thin, 240.1 m, at Ongongo. This compares with an average 385 m (n=11) for all Maieberg sections on the platform, or 370 m (n=9) with the thickest and thinnest (outliers) ignored. From a thermal subsidence model an average sediment accumulation rate of 65 m/Myr was estimated for the Ombaatjie Formation (Halverson *et al*. 2002). This serves as a maximum bound on accumulation rates during the combined Marinoan and Maieberg Formation, yielding a minimum of (370/65) 5.7 Myr duration for Marinoan glaciation and Maieberg deposition combined. If the Maieberg Formation underwent compaction after its accumulation - stylolites are characteristic of upper Tm2 - the minimum combined duration would be longer. Since lithofacies such as tubestone stromatolite (Cloud *et al*. 1974; Corsetti & Grotzinger, 2005; Bosak *et al*. 2013) and benthic crystal fans (Lasaga, 1998; Grotzinger & James, 2000; Vieira *et al*. 2015) imply rapid accumulation for the Maieberg Formation, a multi-million year duration for Marinoan glaciation appeared probable (Hoffman *et al*. 1998a, b). In retrospect, more was learned regarding the fundamental nature of Cryogenian glaciation from the Rasthof and Maieberg cap-carbonate sequences than from the Chuos and Ghaub diamictites.

Elandshoek and Hüttenberg formations (Tsumeb Subgroup)

The base of section P1329a (Fig. 8B) is at 19.1409°S/13.8482°E where the Maieberg-Elandshoek transition (Figs 10 & 11) is a reprise of the Rasthof-Gruis 'catch-up-keep-up' transition (Fig. 5). The basal Te1 member of the Elandshoek Formation (Fig. 11) is a stack of thin (average 2.86 m) regressive cycles, most of which (7 out of 11) end at subaerial exposure surfaces marked by tepees or tepee-breccias above pinkish dolomite microbialaminite. In Te2 and Te3 (Fig. 11), most cycles (40 of 43) end at marine flooding surfaces and only three have evidence of subaerial exposure. As a whole, the Elandshoek Formation is 389 m thick in P1329a (Fig. 8B) and consists of 54 ribbonite-grainstone cycles with an average thickness of 7.2 m. The average thickness is likely overestimated because of cycle undercounting. Cryptic flooding surfaces within grainstone units went unrecorded and stromatolite beds in ribbonite were not counted as cycle boundaries. Member Te2 contains 17 beds (average 0.37 m) of laterally-linked prolate stromatolites ('Tuten', Krüger, 1969), many of which are heavily silicified. The top of the Elandshoek Formation is a prominent flooding surface above an upper member (Te3) dominated by grainstone (Fig. 11).

The base of section P1329b (Fig. 8B) is at 19.1412°S/13.8434°E and the Hüttenberg Formation is divisible into three members (Fig. 12). Th1 is dominated by ribbonite with subordinate stromatolite; Th2 is dominated by marly ribbonite with subordinate ribbonite, and Th3 is dominated by grainstone. There are eight stromatolite beds in Th1, of which the fourth is the thickest (3.3 m) and the average is 1.0 m. Th2 is recessive and the section (Fig. 12) is a composite (Fig. 8B). A 1.4-m-thick silicified bed of laterally-linked stromatolites occurs near the top of Th2. Grainstone in the lower half of Th3 is cross-bedded. A sharp disconformity separates the top of the Hüttenberg Formation from synorogenic foredeep clastics (greywacke semi-pelite) in the Sesfontein Formation of the Mulden Group (Guj, 1970; Hedberg, 1979; SACS, 1980).

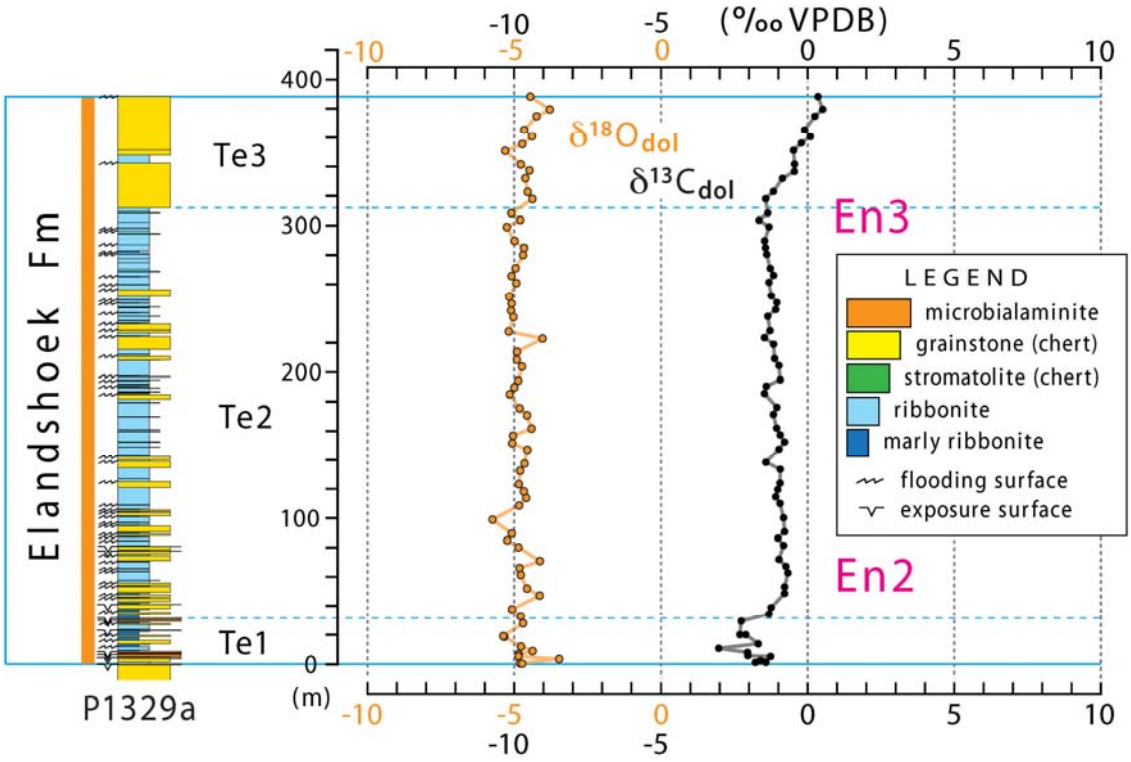

Figure 11. Early Ediacaran Elandshoek Formation (Fig. 1) columnar section P1329a (Fig. 8B) with stable isotope records (Hoffman *et al.* in press). Note offset $\delta^{18}O$ (orange) and $\delta^{13}C$ (black) scales. The formation is divisible into three members Te1-3.

The composite $\delta^{13}C$ record from P9001 and P1329 (Figs 10 & 11) is remarkable in that values remain well below 0.0‰ (VPDB) until the top of the Elandshoek Formation, 605 m above the base of the Ediacaran. This suggests that the Otavi Group platform and the Death Valley area of California (Petterson *et al.* 2011) have the most expanded early Ediacaran sections known (Hoffman *et al.* in press). The positive CIE En4 in the lower-middle Hüttenberg Formation (Fig. 12) is less enriched and prolonged than in correlative strata in the Otavi Mountainland (Cui *et al.* 2018; Hoffman & Lamothe, 2019) but it shares the same large point-to-point variability, the significance of which remains to be revealed and declining accumulation rates alone do not explain.

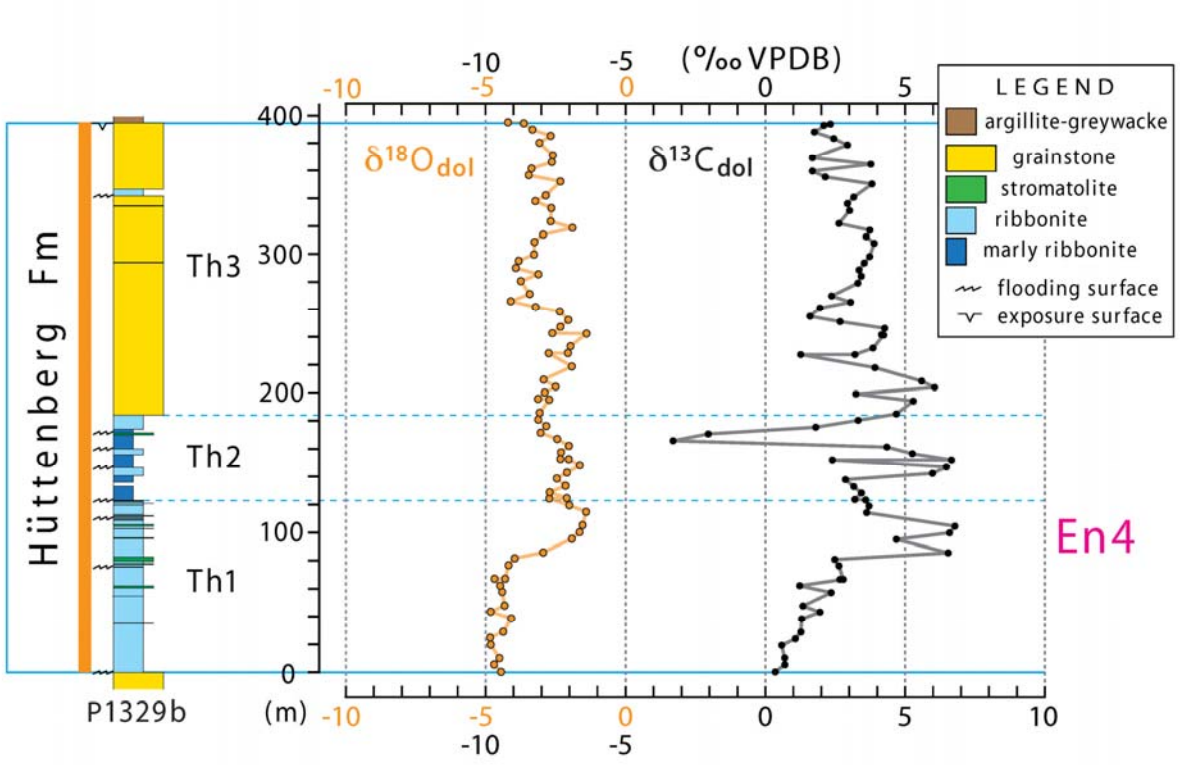

Figure 12. Early Ediacaran Hüttenberg Formation (Fig. 1) columnar section P1329b (Fig. 8B) with stable isotope records (Hoffman *et al*. in press). Note offset $\delta^{18}O$ (orange) and $\delta^{13}C$ (black) scales. The formation is divisible into three members Th1-Th3. CIE En4 is correlated with the Hüttenberg CIE in the northern Otavi Mountainland (Cui *et al*. 2018).

Summary and Discussion

The complete composite section from Ongongo and its $\delta^{18}O$ and $\delta^{13}C$ records are assembled in Figure 13. The Rasthof and Maieberg formations (cap-carbonate sequences) stand out from the other five carbonate formations in their lack of m-scale depositional cycles. This is most easily explained by deep unfilled accommodation generated during the preceding glacial epochs from tectonic subsidence and net erosion. The Cryogenian $\delta^{13}C$ record from the Abenab Subgroup has long been a global standard (Halverson *et al*. 2005, 2010; Halverson & Shields-Zhou, 2011).

A reference section for the Otavi Group in the Eastern Kaoko Zone is not a substitute for one in the Otavi Mountainland. The formation-scale sequences are somewhat different in the two areas (Hedberg, 1979), particularly in the middle Abenab Subgroup. Stable isotope records from the Otavi Mountainland are needed to resolve uncertain correlations of inter-snowball formations between the two areas (Fig. 1). They are also needed to test different interpretations of sub-Marinoan stratigraphic relations-synglacial tectonics in the Otavi Mountainland (Bechstädt *et al*. 2018) or subglacial erosion in the Eastern Kaoko Zone (Hoffman & Halverson, 2008; Hoffman *et al*. in press). Different geology or different interpretations?

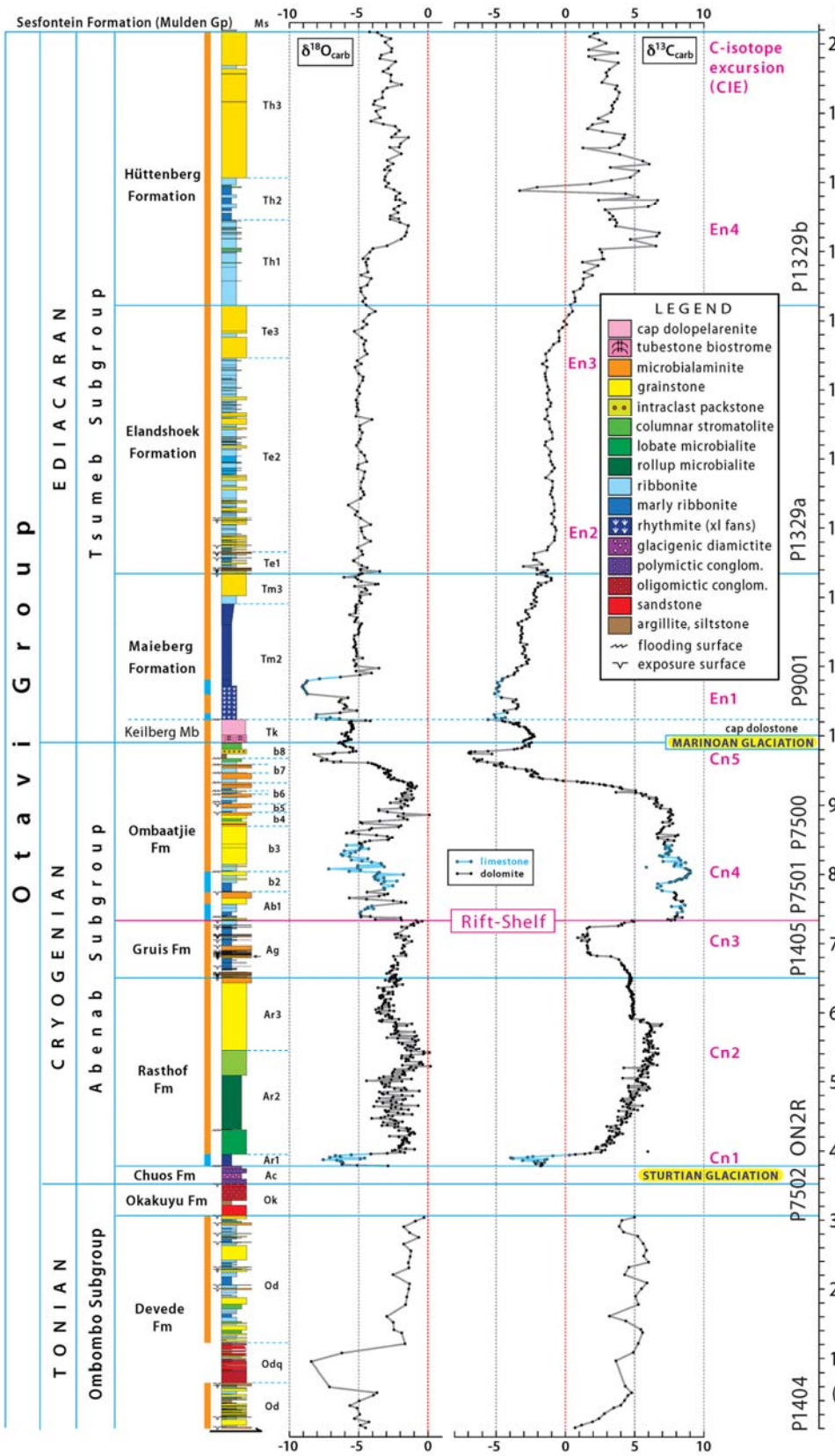

Figure 13. Composite Otavi Group columnar section (Fig. 3) with stable isotope records (tabulated by section number in Hoffman *et al.* in press). The rift-shelf transition is placed after the last major uplift episode of the Huab and Makalani rift shoulders of the outer (southern) platform (Hoffman & Halverson; 2008, Hoffman *et al.* in press). Rift-related structural rotations continued into the late Cryogenian (Marinoan) time in the Swakop Group on the distal foreslope of the Otavi platform and in the Northrn Damara belt (Hoffman *et al.* in press).

Acknowledgements

This research was supported by the Geological Survey of Namibia, Canadian National Science and Engineering Research Council (1993-94), Harvard University (1994-2008), United States National Science Foundation (1995-2008), Canadian Institute for Advanced Research (2010-15) and McGill University (2012-18). Stable isotope measurements, tabulated in Hoffman *et al*. (in press), were obtained in the Laboratory for Geochemical Oceanography at Harvard University directed by Daniel P. Schrag, and in the laboratory of Galen P. Halverson in the Department of Earth and Planetary Sciences at McGill University. Field work was assisted by Peter W. Crockford, Alex de Moor, Eben Blake Hodgin and Glenn Jasechko.

References

Aitken, J.D. 1982. Precambrian of the Mackenzie fold belt - a stratigraphic and tectonic overview. *In:* Hutchison, R.W., Spence, C.D., Franklin, J.M. (Eds) *Precambrian Sulfide Deposits*, *H.S. Robinson Memorial Volume*. Geological Association of Canada Special Paper, **25**, 149-161.

Allen, P.A. & Hoffman, P.F. 2005. Extreme winds and waves in the aftermath of a Neoproterozoic glaciation. *Nature*, **433**, 123-127.

Assereto, R.L.A.M. & Kendall, C.G.StC. 1978. Nature, origin and classification of peritidal tepee structures and related breccias. *Sedimentology*, **24**, 153-210.

Bao, X.J., Zhang, S.H., Jiang, G.Q., Wu, H.C., Li, H.Y., Wang, X.Q., An, Z.Z. & Yang, T.S. 2018. Cyclostratigraphic constraints on the duration of the Datangpo Formation and the onset age of the Nantuo (Marinoan) glaciation in South China. *Earth and Planetary Science Letters*, **483**, 52-63.

Bechstädt, T., Jäger, H., Rittersbacher, A., Schweisfurth, B., Spence, G., Werner, G. & Boni, M. 2018. The Cryogenian Ghaub Formation of Namibia - New insights into Neoproterozoic glaciations. *Earth-Science Reviews*, **177**, 678-714.

Bechstädt, T., Jäger, H., Spence, G. & Werner, G. 2009. Late Cryogenian (Neoproterozoic) glacial and post-glacial successions at the southern margin of the Congo craton, northern Namibia: facies, palaeogeography and hydrocarbon perspective. *In:* Graig, J., Thurow, J., Thusu, B., Thitham, A. & Abutarruma, Y. (Eds) *Global Neoproterozoic Petroleum Systems: The Emerging Potential in North Africa*. Geological Society of London Special Publication, **326**, 255-287.

Bold, U., Crüger Ahm, A.-S., Schrag, D.P., Higgins, J.A., Jamsran, E. & Macdonald, F.A. 2020. Effect of dolomitization on isotopic records from Neoproterozoic carbonates in southwestern Mongolia. *Precambrian Research*, **350**, 105902, 1-19.

Bold, U., Smith, E.F., Rooney, A.D., Bowring, S.A., Buchwaldt, R., Dudás, F.Õ., Ramezani, J., Crowley, J.L., Schrag, D.P. & Macdonald, F.A. 2016. Neoproterozoic stratigraphy of the Zavkhan terrane of Mongolia: the backbone for Cryogenian and early Ediacaran chemostratigraphic records. *American Journal of Science*, **316**, 1-63.

Bosak, T., Lahr, D.J.G., Pruss, S.B., Macdonald, F.A., Dalton, L. & Matys, E. 2011. Agglutinated tests in post-Sturtian cap carbonates of Namibia and Mongolia. *Earth and Planetary Science Letters,* **308**, 29-40.

Bosak, T., Lahr, D.J.G., Pruss, S.B., Macdonald, F.A., Gooday, A.J., Dalton, L. & Matys, E.D. 2012. Possible early foraminiferans in post-Sturtian (716-635 Ma) cap carbonates. *Geology*, **40**, 67-70.

Bosak, T., Mariotti, G., Macdonald, F.A., Perron, J.T. & Pruss, S.B. 2013. Microbial sedimentology in Neoproterozoic cap carbonates. *In:* Bush, A.M., Pruss, S.B. & Payne, J.L. (Eds) *Ecosystem Paleobiology and Geobiology*. Paleontological Society Papers, **19**, 1-25.

Cailteaux, J.L.H. & De Putter, T. 2019. The Neoproterozoic Katanga Supergroup (D. R. Congo): State-of-the-art and revisions of the lithostratigraphy, sedimentary basin and

geodynamic evolution. *Journal of African Earth Sciences*, **150**, 522-531.

Cloud, P., Wright, L.A., Williams, E.G., Diehl, P. & Walter, M.R. 1974. Giant stromatolites and associated vertical tubes from the upper Proterozoic Noonday Dolomite, Death Valley region, eastern California. *Geological Society of America Bulletin*, **85**, 1869-1882.

Corsetti, F.A. & Grotzinger, J.P. 2005. Origin and significance of tube structure in Neoproterozoic post-glacial cap carbonates: example from the Noonday Dolomite, Death Valley, United States. *Palaios*, **20**, 348-362.

Crockford, P.W., Mehra, A., Domack, E.W. & Hoffman, P.F. 2021. Report: An occurrence of radially symmetric sedimentary structures in the basal Ediacaran cap dolostone (Keilberg Member) of the Otavi Group. *Geological Survey of Namibia Communications*, **23**, 26-38.

Cui, H., Kaufman, A.J., Peng, Y.B., Liu, X.M. & Plummer, R.E. 2018. The Neoproterozoic Hüttenberg $\delta^{13}C$ anomaly: Genesis and global implications. *Precambrian Research*, **313**, 242-262.

Dalton, L.A., Bosak, T., Macdonald, F.A., Lahr, D.J.G. & Pruss, S.B. 2013. Preservational and morphological variability of assemblages of agglutinated eukaryotes in Cryogenian cap carbonates of northern Namibia. *Palaios*, **28**, 67-79.

Delpomdor, F., Eyles, N., Tack, L. & Préat, A. 2016. Pre- and post-Marinoan carbonate facies of the Democratic Republic of the Congo: Glacially- or tectonically-influenced deep-water sediments? *Palaeogeography, Palaeoclimatology, Palaeoecology*, **457**, 144-157.

Delpomdor, F., Schröder, S., Préat, A., Lapointe, P. & Blanpied, C. 2018. Sedimentology and chemostratigraphy of the late Neoproterozoic carbonate ramp sequences of the Hüttenberg Formation (northwestern Namibia) and the C5 Formation (western central Democratic Republic of Congo): Record of the late post-Marinoan marine transgression on the margin of the Congo Craton. *South African Journal of Geology*, **121**, 23-42.

Domack, E.W. & Hoffman, P.F. 2011. An ice grounding-line wedge from the Ghaub glaciation (635 Ma) on the distal foreslope of the Otavi carbonate platform, Namibia, and its bearing on the Snowball Earth hypothesis. *Geological Society of America Bulletin*, **123**, 1448-1477.

Dowdeswell, J.A., Hambrey, M.J. & Wu, R.T. 1985. A comparison of clast fabric and shape in Late Precambrian and modern glacigenic sediments. *Journal of Sedimentary Petrology*, **55**, 691-704.

Friedman, I. & O'Neil, J.R. 1977. Compilation of stable isotope fractionation factors of geochemical interest. *In:* Fleischer, M. (Ed.) *Data of Geochemistry, Sixth Edition.* United States Geological Survey Professional Paper, **440-KK**, 1-12 and 49 figures.

Goscombe, B., Foster, D.A., Gray, D. & Wade, B. 2018. The evolution of the Damara orogenic system: A record of West Gondwana assembly and crustal response. *In:* Siegesmund, S., Basei, M.A.S., Oyhantçabal, P. & Oriolo, S. (Eds) *Geology of Southwest Gondwana*. Springer International, Berlin, pp. 303-352.

Gradstein, F.M., Ogg, J.G., Schmitz, M.D. & Ogg, G.M. 2012. *The Geologic Time Scale 2012*. Elsevier, Amsterdam, 1176 pp.

Grotzinger, J.P. & James, N.P. 2000. Precambrian carbonates: evolution of understanding. *In:* Grotzinger, J.P. & James, N.P. (Eds) *Carbonate Sedimentation and Diagenesis in the Evolving Precambrian World*. SEPM (Society for Sedimentary Geology) Special Publication, **67**, 3-20.

Guj, P. 1970. The Damara Belt in the south-western Kaokoveld, South West Africa. *University of Cape Town Precambrian Research Unit Bulletin*, **8**, 168 pp. + 4 map sheets (scale 1:125,000) + cross-sections.

Hedberg, R.M. 1979. Stratigraphy of the Ovamboland Basin, South West Africa. *University of Cape Town Precambrian Research Unit Bulletin*, **24**, 325 pp. + 6 map sheets (scale 1:250,000).

Hegenberger, W. 1987. Gas escape structures in Precambrian peritidal carbonate rocks. *Communications of the Geological Survey of Namibia*, **3**, 49-55.

Halverson, G.P., Hoffman, P.F., Schrag, D.P. & Kaufman, A.J. 2002. A major perturbation of the carbon cycle before the Ghaub glaciation (Neoproterozoic) in Namibia: Prelude to snowball Earth? *Geochemistry Geophysics Geosystems*, **3**, doi: 10.1029/2001GC000244.

Halverson, G.P., Hoffman, P.F., Schrag, D.P., Maloof, A.C. & Rice, A.H.N. 2005. Toward a Neoproterozoic composite carbon-isotope record. *Geological Society of America Bulletin*, **117**, 1181-1207.

Halverson, G.P. & Shields-Zhou, G. 2011. Chemostratigraphy and the Neoproterozoic glaciations. *In:* Arnaud, E., Halverson, G.P. & Shields-Zhou, G. (Eds) *The Geological Record of Neoproterozoic Glaciations*. Geological Society of London Memoir, **36**, pp. 51-66.

Halverson, G.P., Wade, B.P., Hurtgen, M.T. & Barovich, K.M. 2010. Neoproterozoic chemostratigraphy. *Precambrian Research*, **182**, 337-350.

Hoffman, P.F. 2011a. Glacigenic and associated strata of the Otavi carbonate platform and foreslope, northern Namibia: evidence for large base-level and glacioeustatic changes. *In:* Arnaud, E., Halverson, G.P., Shields-Zhou, G. (Eds) *The Geological Record of Neoproterozoic Glaciations*. Geological Society of London Memoir, **36**, 195-209.

Hoffman, P.F. 2011b. Strange bedfellows: glacial diamictite and cap carbonate from the Marinoan (635 Ma) glaciation in Namibia. *Sedimentology*, **58**, 57-119.

Hoffman, P.F. & Halverson, G.P. 2008. Otavi Group of the western Northern Platform, the eastern Kaoko Zone and the western Northern Margin Zone. *In:* Miller, R. McG. (Ed.) *The Geology of Namibia, Vol. 2*. Geological Survey of Namibia, pp. 13.69-13.136.

Hoffman, P.F., Halverson, G.P., Domack, E.W., Husson, J.M., Higgins, J.A. & Schrag, D.P. 2007. Are basal Ediacaran (635 Ma) post-glacial "cap dolostones" diachronous? *Earth and Planetary Science Letters*, **258**, 114-131.

Hoffman, P.F. Halverson, G.P., Schrag, D.P., Higgins, J.A., Domack, E.W., Macdonald, F.A., Pruss, S.B., Blättler, C.L., Crockford, P.W., Hodgin, E.B., Bellefroid, E.J., Johnson, B.W., Hodgskiss, M.S.W., Lamothe, K.G., LoBianco, S.L.C., Busch, J.F., Howes, B.J., Greenman, J.W., Nelson, L.L., In press. Snowballs in Africa: sectioning a long-lived Neoproterozoic carbonate platform and its bathyal foreslope (NW Namibia). *Earth-Science Reviews*. https://doi.org/10.1016/j.earscirev.2021.103616.

Hoffman, P.F., Kaufman, J.A. & Halverson, G.P. 1998a. Comings and goings of global glaciations on a Neoproterozoic carbonate platform in Namibia. *GSA Today*, **8**, 1-9.

Hoffman, P.F., Kaufman, A.J., Halverson, G.P. & Schrag, D.P. 1998b. A Neoproterozoic snowball Earth. *Science*, **281**, 1342-1346.

Hoffman, P.F., Lamothe, K.G. & Greenman, J.W. 2018. Report: Stratigraphic investigations of the Neoproterozoic Otavi/Swakop Group in the southern Kunene Region. *Communications of the Geological Survey of Namibia*, **20**, 100-113.

Hoffmann, K.-H. & Prave, A.R. 1996. A preliminary note on a revised subdivision and regional correlation of the Otavi Group based on glaciogenic diamictites and associated cap dolomites. *Communications of the Geological Survey of Namibia*, **11**, 77-82.

Hofmann, H.J., 1969. Attributes of stromatolites. *Geological Survey of Canada Paper*, **69-39**, 58 pp.

Johnston, D.T., Macdonald, F.A., Gill, B.C., Hoffman, P.F. & Schrag, D.P. 2012. Uncovering the Neoproterozoic carbon cycle. *Nature*, **483**, 320-323.

Kadima, E., Delvaux, D., Sebagenzi, S.N., Tack, L. & Kabeya, S.M. 2011. Structure and geological history of the Congo Basin: an integrated interpretation of gravity, magnetic and reflection seismic data. *Basin Research*, **23**, 499-527.

Kamona, A.F. & Günzel, A. 2007. Stratigraphy and base metal mineralization in the Otavi Mountain Land, Northern Namibia - a review and regional interpretation. *Gondwana Research*, **11**, 396-413.

Kaufman, A.J., Hayes, J.M., Knoll, A.H. & Germs, G.J.B. 1991. Isotopic compositions of carbonates and organic carbon from upper Proterozoic successions in Namibia: stratigraphic variation and the effects of diagenesis and metamorphism. *Precambrian Research*, **49**, 301-327.

Kaufman, A.J., Knoll, A.H. & Narbonne, G.M. 1997. Isotopes, ice ages, and terminal Proterozoic earth history. *Proceedings of the U.S. National Academy of Sciences*, **94**, 6600-6605.

Kendall, G.St.C. & Warren, J. 1987. A review of the origin and setting of tepees and their

associated fabrics. *Sedimentology*, **34**, 1007-1027.

King, C.H.M. 1994. Carbonates and mineral deposits of the Otavi Mountainland. *Geological Survey of Namibia International Conference on Proterozoic Crustal & Metallogenic Evolution Excursion*, **4**, 40 pp.

Knoll, A.H., Walter, M.R., Narbonne, G.M. & Christie-Blick, N. 2006. The Ediacaran Period: a new addition to the geologic time scale. *Lethaia*, **39**, 13-30.

Krüger, L. 1969. Stromatolites and oncolites in the Otavi Series, South West Africa. *Journal of Sedimentary Petrology*, **39**, 1046-1056.

Lan, Z.W., Huyskens, M.H., Lu, K., Li, X.H., Zhang, G.Y., Lu, D.B. & Yin, Q.Z. 2020. Toward refining the onset age of Sturtian glaciation in South China. *Precambrian Research*, **338**, 105555, 1-8.

Lasaga, A. 1998. *Kinetic Theory in the Earth Sciences*. Princeton University Press, NJ. 822 pp.

Le Ber, E., Le Heron, D.P., Winterleitner, G., Bosence, D. & Vining, B.A. 2013. Microbial-ite recovery in the aftermath of the Sturtian glaciation: Insights from the Rasthof Formation, Namibia. *Sedimentary Geology*, **294**, 1-12.

Lehmann, J., Saalmann, K., Naydenov, K.V., Milani, L., Belyanin, G.A., Zwingmann, H., Charlesworth, G. & Kinnaird, J.A. 2016. Structural and geochronological constraints on the Pan-African tectonic evolution of the northern Damara Belt, Namibia. *Tectonics*, **35**, 103-135.

Lokier, S.W., Andrade, L.L., Court, W.M., Dutton, K.E., Head, I.M., van der Land, C., Paul, A. & Sherry, A. 2018. A new model for the formation of microbial polygons in a coastal sabkha setting. *Depositional Record*, **3**, 201-208.

Macdonald, F.A., Schmitz, M.D., Strauss, J.V., Halverson, G.P., Gibson, T.M., Eyster, A., Cox, G., Mamrol, P. & Crowley, J.L. 2018. Cryogenian of Yukon. *Precambrian Research*, **319**, 114-143.

MacLennan, S., Park, Y., Swanson-Hysell, N., Maloof, A., Schoene, B., Gebreslassie, M, Antilla, E., Tesema, T., Alene, M. & Haileab, B. 2018. The arc of the Snowball: U-Pb dates constrain the Islay anomaly and the initiation of the Sturtian glaciation. *Geology*, **46**, 539-542.

Miller, R.McG. 2008b. *The Geology of Namibia: Vol. 2, Neoproterozoic to Lower Palaeozoic*. Geological Survey of Namibia, Windhoek.

Miller, R.McG. 2013. Comparative stratigraphic and geochronological evolution of the Northern Damara Supergroup in Namibia and the Katanga Supergroup in the Lufilian Arc of Central Africa. *Geoscience Canada*, 40, http://dx.doi.org/10.12789/geocanj.2013.40.007

Moore, K.R., Bosak, T., Macdonald, F.A., Lahr, D.J.G., Newman, S., Settens, C. & Pruss, S.B. 2017. Biologically agglutinated eukaryotic microfossil from Cryogenian cap carbonates. *Geobiology*, **15**, 499-515.

Narbonne, G.M., Xiao, S.H. & Shields, G.A. 2012. The Ediacaran Period. *In:* Gradstein, F.M., Ogg, J.G., Schmitz, M.D. & Ogg, G.M. (Eds) *The Geologic Time Scale 2012*. Elsevier, Amsterdam, pp. 413-435.

Nelson, L.L., Smith, E.F., Hodgin, E.B., Crowley, J.L., Schmitz, M.D. & Macdonald, F.M. 2021. Geochronological constraints on Neoproterozoic rifting and onset of the Marinoan glaciation from the Kingston Peak Formation in Death Valley, California (USA). *Geology*, **48**, https://doi.org/10.1130/G47668.1

Nogueira, A.C.R., Riccomini, C., Sial, A.N., Moura, C.A.V., Trindade, R.I.F. & Fairchild, T.R. 2007. Carbon and strontium isotope fluctuations and paleoceanographic changes in the late Neoproterozoic Araras carbonate platform, southern Amazon craton, Brazil. *Chemical Geology*, **237**, 168-190.

Partin, C.A. & Sadler, P.M. 2016. Slow net sediment accumulation sets snowball Earth apart from all younger glacial episodes. *Geology*, **44**, 1019-1022.

Petterson, R., Prave, A.R., Wernicke, B.P. & Fallick, A.E. 2011. The Neoproterozoic Noonday Formation, Death Valley region, California. *Geological Society of America Bulletin*, **123**, 1317-1336.

Pillans, B. & Gibbard, P. 2012. The Quaternary Period. *In:* Gradstein, F.M., Ogg, J.G., Schmitz, M.D. & Ogg, G.M. (Eds) *The Geologic Time Scale 2012, Vol. 2*. Elsevier, Amsterdam, pp. 979-1010.

Prave, A.R., Condon, D.J., Hoffmann, K.-H., Tapster, S. & Fallick, A.E. 2016. Duration and nature of the end-Cryogenian (Marinoan) glaciation. *Geology*, **44**, 631-634.

Preiss, W.V. & Forbes, B.G. 1981. Stratigraphy, correlation and sedimentary history of Adelaidean (Late Proterozoic) basins in Australia. *Precambrian Research*, **15**, 255-304.

Pruss, S.B., Bosak, T., Macdonald, F.A., McLane, M. & Hoffman, P.F. 2010. Microbial facies in a Sturtian cap carbonate, the Rasthof Formation, Otavi Group, northern Namibia. *Precambrian Research*, **181**, 187-198.

Rooney, A.D., Strauss, J.V., Brandon, A.D. & Macdonald, F.A. 2015. A Cryogenian chronology: Two long-lasting synchronous Neoproterozoic glaciations. *Geology*, **43**, 459-462.

Rooney, A.D., Yang, C., Condon, D.J., Zhu, M.Y. & Macdonald, F.A. 2020. U-Pb and Re-Os geochronology tracks stratigraphic condensation in the Sturtian snowball aftermath. *Geology*, **48**, 625-629.

Rose, C.V., Swanson-Hysell, N.L., Husson, J.M., Poppick, L.N., Cottle, J.M., Schoene, B. & Maloof, A.C. 2012. Constraints on the origin and relative timing of the Trezona $\delta^{13}C$ anomaly below the end-Cryogenian glaciation. *Earth and Planetary Science Letters,* **319-320**, 241-250.

SACS (South African Committee for Stratigraphy) 1980. Damara Sequence. *In:* Kent, L.E. (Ed.) *Stratigraphy of South Africa Part 1: Lithostratigraphy of the Republic of South Africa, South West Africa/Namibia and the Republics of Bophuthatswana, Transkei and Venda*. Geological Survey of South Africa Handbook, **8**, pp. 415-438.

Schlager, W. 2005. Carbonate Sedimentology and Sequence Stratigraphy. *SEPM (Society for Sedimentary Geology) Concepts in Sedimentology and Paleontology*, **8**, 200 pp.

Shields-Zhou, G.A., Porter, S. & Halverson, G.P. 2016. A new rock-based definition for the Cryogenian Period (circa 720 - 635 Ma). *Episodes*, **39** (**1**), 3-8.

Söhnge, P.G. 1953. Review of the geology of the Otavi Mountain Land, South West Africa. Unpublished Report, Tsumeb Corporation Ltd, Tsumeb.

Söhnge, P.G., 1957. Revision of the geology of the Otavi Mountainland, South West Africa (with 1958 amended stratigraphic table). Unpublished Report, Tsumeb Corporation Ltd, Tsumeb.

Tziperman, E., Halevy, I., Johnston, D.T., Knoll, A.H. & Schrag, D.P. 2011. Biologically induced initiation of Neoproterozoic snowball-Earth events. *Proceedings of the U.S. National Academy of Sciences*, **108** (**37**), 15,091-15,096.

Vieira, L.C., Nédélec, A., Fabre, S., Trindade, R.I.F. & Paes de Almeida, R. 2015. Aragonite crystal fans in Neoproterozoic cap carbonates: a case study from Brazil and implications for the post-snowball Earth coastal environment. *Journal of Sedimentary Research*, **85**, 285-300.

Wallace, M.W., Hood, A.v.S., Woon, E.M.S., Hoffmann, K.-H. & Reed, C.P. 2014. Enigmatic chambered structures in Cryogenian reefs: The oldest sponge-grade organisms? *Precambrian Research*, **255**, 109-123.

Watts, A.B., Karner, G.D. & Steckler, M.S. 1982. Lithospheric flexure and the evolution of sedimentary basins. *Philosophical Transactions of the Royal Society of London Series A*, **305** (**1489**), 249-281.

Zhou, C.M., Huysken, M.H., Lang, X.G., Xiao, S.H. & Yin, Q.Z. 2019. Calibrating the terminations of Cryogenian global glaciations. *Geology*, **47**, 251-254.